Using Magnetism to Characterize and Distinguish High Coercivity Iron Oxide and Oxyhydroxide Minerals in Atmospheric Dust

A thesis
Submitted to the faculty of
University of Minnesota
By

Kimberly E. Yauk

In partial fulfillment of the requirements
For the degree of
Master of Science

Bruce M. Moskowitz

July 2013

Acknowledgements

One of the best aspects of my graduate career has been the guidance, collaboration, and support I have had with mentors and colleagues along the way. I would first like to thank my advisor, Bruce Moskowitz, without whom this research would not be possible. His patience explaining the fundamentals of magnetism has been immeasurably helpful in introducing me to this field, and it was his support that made my research possible.

I am grateful for all the help I received from the rest of the personnel of the Institute for Rock Magnetism. Mike Jackson, Julie Bowles, Peat Solheid, and Dario Bilardello all helped answer my endless questions and trouble shoot machine problems. Subir Banerjee's encouragement and first review of my thesis was instrumental. Thank you to Josh Feinberg and Lee Penn for serving on my graduate committee.

I would also like to thank those from other institutions for providing their expertise. The enthusiasm of Rich Reynolds along with the contributions by the USGS-Denver brought this project to the Institute for Rock Magnetism. Special thanks go to Ramon Egli (Munich University, Department of Geophysics) for his guidance using the MagMix program and his technical assistance. And to Thelma Berquó (Concordia University, Moorhead, MN) for her work fitting Mössbauer spectra.

Lastly, thank you to my family and friends for their support and offers to read through my thesis. Thanks also for the work done by intern Chelsea Ottenfeld measuring samples last summer.

Abstract

Natural atmospheric dust samples collected from the American southwest and globally were measured using magnetic methods in order to separate remanence attributed to the high coercivity iron oxide and oxyhydroxide minerals hematite and goethite. Dust collected from mountain snow and dust source areas in nearby arid plains were analyzed using traditional room- and low temperature methods. Additional methods were created to better examine the weak, high coercivity components. Combinations of high fields (2.5-9 T), low temperatures (10-300 K), partial AF demagnetization, and thermal demagnetization to 400 K were implemented to separate each component. Percentages of remanence attributed to magnetite, hematite, and goethite were compared to results found by HIRM (hard isothermal remanent magnetization) and Mössbauer spectroscopy with good correlation and to coercivity unmixing methods without correlation. TRM (thermoremanent magnetization) was found to be an important step in magnetizing a greater portion of the goethite fraction. Further procedures for characterizing nano grain sizes would be illuminating.

Table of Contents

List of Tables

List of Figures

Introduction:

Dust is an important component of the atmosphere deserving a thorough study because it controls many of the global systems that impact human life. Dust storms deliver nutrients such as phosphorus and iron through sediment transport to agricultural plots on land and to phytoplankton communities in the ocean (Anderson and Downing, 2006; Engelbrecht and Derbyshire, 2010; Gassó et. al., 2010). When respired, dust directly affects human health by blocking and irritating lung tissue and by introducing heavy metals and radioactive particles to the body (Galloway et. al. 1982; Plumlee and Ziegler, 2003). Dust in the air can alter ice formation and cloud nucleation, which influence the pattern of rainfall (Gassó et. al., 2010). Lastly, dust particles in the air and on earth surfaces absorb and reflect solar radiation, affecting climate both regionally and globally (Alfaro et. al., 2004).

The snow-covered mountains of the American Southwest experience dust storms every winter and spring, accumulating 5-10 grams per square meter per year from 2004-2008 (Lawrence et. al., 2010). Dust on snow reduces albedo, leading to increased absorption of solar infrared (IR) radiation. This enhanced absorption due to dust loading, termed radiative forcing, leads to an average of 25-50 W/m^2 of extra energy in the snow of the Upper Colorado River Basin (UCRB) over spring melt months, causing snow melt to peak three weeks earlier

than it would otherwise (Painter et. al., 2010). Early springtime melt due to IR absorption causes drought conditions by the late summer months.

The Colorado River Basin, covering approximately 246,000 square miles across Arizona, California, Colorado, Nevada, New Mexico, Utah, and Wyoming, is home to over 27 million people and contains over 4 million acres of cropland (Painter et. al., 2010). This vast area is frequently affected by early spring run-off and overallocation, resulting in water shortages.

In the past, atmospheric dust was not recognized as a contributing factor in climate patterns and so was not taken into account in climate models. It is now known that dust is vital to climate modeling for its role in IR absorption and heat transfer. Atmospheric climate models have been produced to estimate the timing and magnitude of runoff due to radiative forcing in the UCRB over a period from 1916-2003 using the Variable Infiltration Capacity model (Painter et. al., 2010). Initial studies of dust composition along with satellite images have shown that dust storms appear to be localized, drawing sediments from nearby arid plains (Lawrence et. al., 2010). The model based findings on dust trajectories using geostationary remote sensing and isotopic analysis (Painter et. al., 2007).

Reflectance spectroscopy was carried out on atmospheric dust samples using a halogen light source over wavelengths in the visible to IR range in order to monitor albedo and identify components of dust that have the greatest impact on climate through heat absorption. Iron oxide minerals, particularly hematite

and goethite, were responsible by far for the majority of IR absorption. In order to better model heat absorption and reflection, more data are needed to define specific mineral content in atmospheric dust. With information on precise mineralogies and grain sizes that affect albedo, atmospheric models will better forecast expected snowmelt and lead to more informed water resource management in an area with such a dearth of rainfall.

The USGS collected atmospheric dust on snowpack (DOS) in the Wasatch Mountains near Salt Lake City, Utah (2010), and the San Juan Mountain Range near Boulder, Colorado (2005-2011). Possible dust source areas (DSAs) identified from satellite imagery taken during dust storms were also sampled in order to compare dust origins. DOS in the San Juan Mountains is believed to be localized in origin due to the high content of silt- and clay-sized particles (Lawrence et. al., 2010). Initial reflectivity data run by the USGS on DOS samples identified hematite and goethite as primary IR absorbers but did not have the sensitivity to precisely estimate mineral percentages.

Magnetic measurements were then requested to assess the composition and concentration of the hematite and goethite. Magnetic measurements of bulk samples are ideal because they require very little sample material (<200 mg), can detect magnetic minerals down to very small amounts (<0.1 wt %), are simple, inexpensive, and, because they are measured in bulk, prevent any separation step or sample biasing. Additionally, measurements do not involve safety

concerns due to harsh chemicals or radioactive materials. The Institute for Rock Magnetism of the University of Minnesota was asked to measure and characterize the iron oxide minerals. The majority of the magnetic measurements from this study were performed there while some were also done at USGS-Denver.

In Sydney, New South Wales (NSW), Australia, a record-breaking dust storm swept through the city on September 23rd, 2009 along a 3000 km front, reducing visibility to 400 meters for close to four hours (Leys, 2011). Particulate matter concentrations exceeded 15,000 um/m^3 while normal levels are <20 ug/m^3 (Engelbrecht and Derbyshire, 2010). Advance warning of the storm allowed local researchers to place dust collection traps and to monitor changes in the dust composition as the storm progressed across the state. These dust samples will show how two critically important iron oxide minerals, hematite and goethite, vary as they are carried downwind along with possible additions of locally derived anthropogenic sources.

This study intends to identify and quantify the iron oxide minerals in bulk specimens from atmospheric dust sampled around the globe in order to provide detailed input data for climate models. Specifically, the study focuses on finding feasible and relatively convenient methods of differentiating the high coercivity

hematite and goethite minerals in bulk natural samples using magnetometers and Mössbauer spectrometers over a range of temperatures (4-400 K) and field strengths (0-9 T) without destroying the sample or separating the magnetic components. Different magnetic measurements will reveal specific aspects about grain size and composition that together will create an idea of the overall dust composition. A secondary goal of the study is to apply the new knowledge to a limited, but specific problem: to compare DOS to DSA and trace origins of the DOS through correlations of magnetic parameters.

Section 1 will briefly summarize types of magnetization and introduce magnetite, hematite and goethite as the three main magnetic minerals. Sections 2 and 3 will give methods and results followed by a discussion of the findings and conclusions in sections 4 and 5. An appendix at the end provides full tables of results.

1 Background

1.1 Introduction to Rock Magnetism

Rock magnetism is the study of magnetic mineral grains contained in a rock sample. Samples are characterized by their (a) remanence, or ability to carry magnetization after exposure to a field, and (b) susceptibility, or tendency to be affected by an applied magnetic field. The study of rock magnetism can be used to identify and quantify iron oxide and oxyhydroxide minerals (from here on simply referred to as "iron oxide minerals") in a bulk sample composed otherwise of paramagnetic and diamagnetic minerals like quartz, feldspars, and clays.

Of the three main types of magnetism, rock magnetic studies focus on ferromagnetism, which includes ferri- and antiferromagnetism. Ferromagnetic substances retain a magnetic moment (remanence) after an applied external field is removed. The moment results from atoms with unpaired electron spins exchange coupled parallel to each other, creating a cooperative magnetic moment in one direction. Ferromagnetism is mostly carried by metals and alloys of iron, nickel, and cobalt (Evans and Heller, 2003). Ferrimagnetism is common in iron-bearing minerals, mainly oxides and sulfides, and has unpaired electrons coupled parallel and antiparallel, with one direction favored, creating a magnetic

moment in the favored direction. Antiferromangetism has no net moment due to complete cancellation of parallel and antiparallel electron moments. However, because of the nature of minerals, antiferromagnetic crystal structures usually contain defects such as ion substitution or vacancies, which fail to cancel and result in a small net magnetic moment that is weak but very stable.

As temperatures rise, thermal fluctuations increase, destabilizing the moment and causing grains to overcome energy barriers that result in magnetic moments freely spinning. Above these temperatures, magnetic particles become paramagnetic and lose ferromagnetic behavior, bringing remanence to zero. The temperatures at which magnetic ordering is lost is called the Curie temperature (T_C) and is specific to individual minerals.

Grain size is a major factor that determines how a magnetic grain will hold remanence. To reach the lowest energy state, larger grains may spontaneously divide their internal magnetic moments into regions with moments in opposite directions called domains. The actual size at which grains become multi-domain (MD) depends on the purity of the mineral, shape of the grain, and strength of magnetic moment (Kneller and Luborsky, 1963; Dunlop, 1973; Butler and Banerjee, 1975). In magnetite, transition from single domain (SD) to MD is estimated to be between 0.1-1 um. Higher coercivity minerals like hematite and goethite have much weaker magnetic strengths and so have stable SD grains at larger sizes with SD/MD transitions occurring in hematite at ~15

um (Banerjee, 1971; Chevallier and Mathieu, 1943). The domains of a MD grain will cancel and nullify the internal magnetic field, resulting in no net, or very weak, remanence of the grain. In contrast, SD grains are too small to have domain walls and result in magnetic moments in one single direction, carrying remanence. They are the most sought-after grain size in magnetic measurements for their high remanence and stability. The size of SD grains of magnetite ranges from ~25 nm to a few hundred nm (McNab et. al., 1968; Dunlop, 1972). Pseudo-single domain **(**PSD) grains, first proposed by Stacey (1962) are grain sizes in the MD range but that display characteristics of SD grains. Superparamagnetic (SP) grains are small enough that they are perturbed by thermal energy and cannot hold remanence. When cooled, SP grains will eventually lose that energy and become magnetically ordered. The temperature transition at which grains become ordered is called the blocking temperature (T_B) and is unique for individual grains. Once blocked, SP grains will carry remanence.

1.2 Iron Oxide Minerals

Magnetite (Fe_3O_4) is the most commonly studied mineral in magnetism due to its strong magnetic signal and trace concentration in many earth materials. Magnetite is a ferrimagnetic mineral most commonly found in mafic igneous and metamorphic rocks and as inclusions in silicate rocks. In sediments,

magnetite is widespread and comes from eroded materials or is made as a by-product by some microorganisms. With a magnetic moment hundreds of times greater than hematite or goethite, magnetite is magnetically stronger than most iron oxide and sulfide minerals, making it easy to detect. Even fractions of a weight percent can overwhelm the signal of other iron oxide minerals present in a sample. Magnetite has a low coercivity, making it magnetically "soft," which allows it to magnetically saturate in fields well below 1 Tesla. Magnetite undergoes a characteristic phase transition at 120 K called the Verwey transition in which the crystalline structure changes from cubic to monoclinic (Özdemir and Dunlop, 1999). In natural samples, the temperature of the Verwey transition (T_V) may be lowered through cation substitution or small grain size. (Aragón et. al., 1985; Moskowitz et. al., 1998)

Goethite (FeOOH) is a common weathered product in soils and loesses. It occurs in moist, acidic soils (Schwertmann and Taylor, 1989), is brown to yellow in color, and is antiferromagnetic with a defect moment imparting weak magnetism (Dunlop, 1971). Goethite has a very high coercivity, meaning that it does not become magnetically saturated until very high fields are applied. Indeed, in some experiments, researchers have pulsed samples of natural goethite in fields as high as 57 Tesla and still not reached saturation (Rochette et. al., 2005). It is unknown if these goethite samples even have a saturation limit or if their internal magnetic order changes as magnetic fields get progressively

higher (Rochette et. al., 2005). This same study did find, however, other synthetic goethite samples that are saturated by approximately 20 T. The coercivity of goethite is higher than hematite and so will require the highest fields to saturate. Maher (2004) found that hematite is 62-73% saturated in a 2T field while goethite gains 84-92% of its remanence between 2 and 7 tesla and is still not near saturation. Goethite has no low temperature transitions. Instead, goethite shows a characteristic linear monotonic increase in remanence as temperature decreases with an applied field (Dekkers, 1989; France and Oldfield, 2000). The Curie temperature (T_C) of goethite is 393 K, which is closer to room temperature than other iron oxide minerals. Observations of monotonic increases in remanence at low temperature along with a sharp drop in remanence on heating to 400 K are indications of the presence of goethite.

Hematite (Fe_2O_3) is very common in hot, dry soils (Schwertmann and Taylor, 1989) and imparts its sediments with red color. A highly oxidized antiferromagnetic mineral, hematite has only ferric ions which derive their magnetic moment at room temperature (300 K) from canted electron spins orders of magnitude lower than magnetite. Hematite undergoes a characteristic phase transition at ~260 K called the Morin transition (Morin, 1950). Below this temperature (T_M), electron spin moments flip to align parallel to the C axis of the mineral, causing a large change in remanence that can be seen on cooling. Suppression of the Morin transition can be due to Ti-substitution (Haigh, 1957)

or very small grain sizes under 0.03 um (Bando et. al., 1965). Like goethite, hematite has a high coercivity and will only saturate in high fields (~2 Tesla) (Dunlop, 1971; Maher et. al., 2004).

Hematite and goethite are both high coercivity minerals, which make them difficult to distinguish using standard magnetic measurements. Because of their roles as radiative absorbers, hematite and goethite are important minerals to differentiate.

1.3 Sample Locations

Samples from the American southwest were collected from Colorado, Arizona, Utah, New Mexico, and Nevada. Dust-on-snow (DOS) sites were located in the Wasatch Mountains near Salt Lake City, Utah and the San Juan Mountains in Colorado (SASP and R0). Three more DOS samples, Shrine, Niwot Ridge, and Boulder, were collected from around Denver. The possible dust source areas (DSA) for the Wasatch Mountains were sampled in Milford Fire Flats (MFF) and Sevier Lake in Utah. Additional samples were collected from an ATV sporting ground in Nellis, Nevada. The possible DSA sites for the San Juan Mountains were collected from Chinle Valley and the Little Colorado River (LCR) in northeastern Arizona and from Twin Lakes in the northwest of New Mexico.

The Australian samples were collected ahead of the Red Dawn dust storm in a path that traced the storm downwind. Two samples, F5 and F6, were located upwind of the Cowal Gold Mine (Lake Eyre Basin in western New South Wales) from agricultural fields with solis described as red chromosols (Cattle et al., 2012) of the. Samples F1-F4 were located progressively downwind from the gold mine across a dried lakebed made of gray lacustrian sediments. The Orange sample was an intermediate location in the central west region of New South Wales 158 miles west of Sydney. Three samples were collected in smaller amounts from the Sydney area itself including the roof of the University of Sydney library (Fisher) and suburbs of St. Peters to the west and Hornsby to the north.

Additional samples were given to the Institute for Rock Magnetism for global comparison. These African samples include three samples from the Kalahari Desert and thirteen from the Bodele depression in northern Chad. The Kalahari and Bodele samples were given to the USGS by Charlie Bristow of the University of London. Four Bodele samples were sieved to the 125-2000 um size. Those same four and five others were once more separated down to the 63 um range.

Synthetic samples were measured for comparison with particular emphasis on nano-sized grains. Three hematite, two goethite, and one maghemite samples were measured. Hematite and maghemite synthetic "Skyspring" 20-40 nm standards were given by Rich Reynolds at the USGS in Denver. Two nano-size

standards, a 10x100 nm goethite and a 25 nm hematite were given by the chemistry department of the University of Minnesota. Lastly, WS222 goethite standard represents a thin coat of goethite grains on larger silicate minerals, and GDS27 is a hematite standard, both given by the USGS because they most closely matched reflectivity measurements.

2 Methods

2.1 Sample Collection:

The American Southwest samples were all collected by the USGS between 2005 and 2011. See Figure 2-1 for collection locations. DOS samples were collected after a period of ablation when dust had accumulated on the top of snow in a layer. Centimeter deep snow grids of 0.75 meter squares were carved out of the surface and later melted to isolate the dust particles. Dust source sediments were collected from both the ground and passive air filters set from 0.5 to 100 cm off the ground. Filters were emptied every four months or sooner as needed. Dust samples were sieved to less than 63 microns and additionally to less than 20 microns for Little Colorado River samples. Two samples (Tucker Flat 3 and Stop 15 Tyende Court) were sieved again down to particle size PM10 (10 um). Australia samples were collected both opportunistically from large surfaces in the city of Sydney and systematically in inverted Frisbee dust gauges in the Lake Cowel region after the dust storm on September 22nd-23rd 2009 (Figure 2-2).

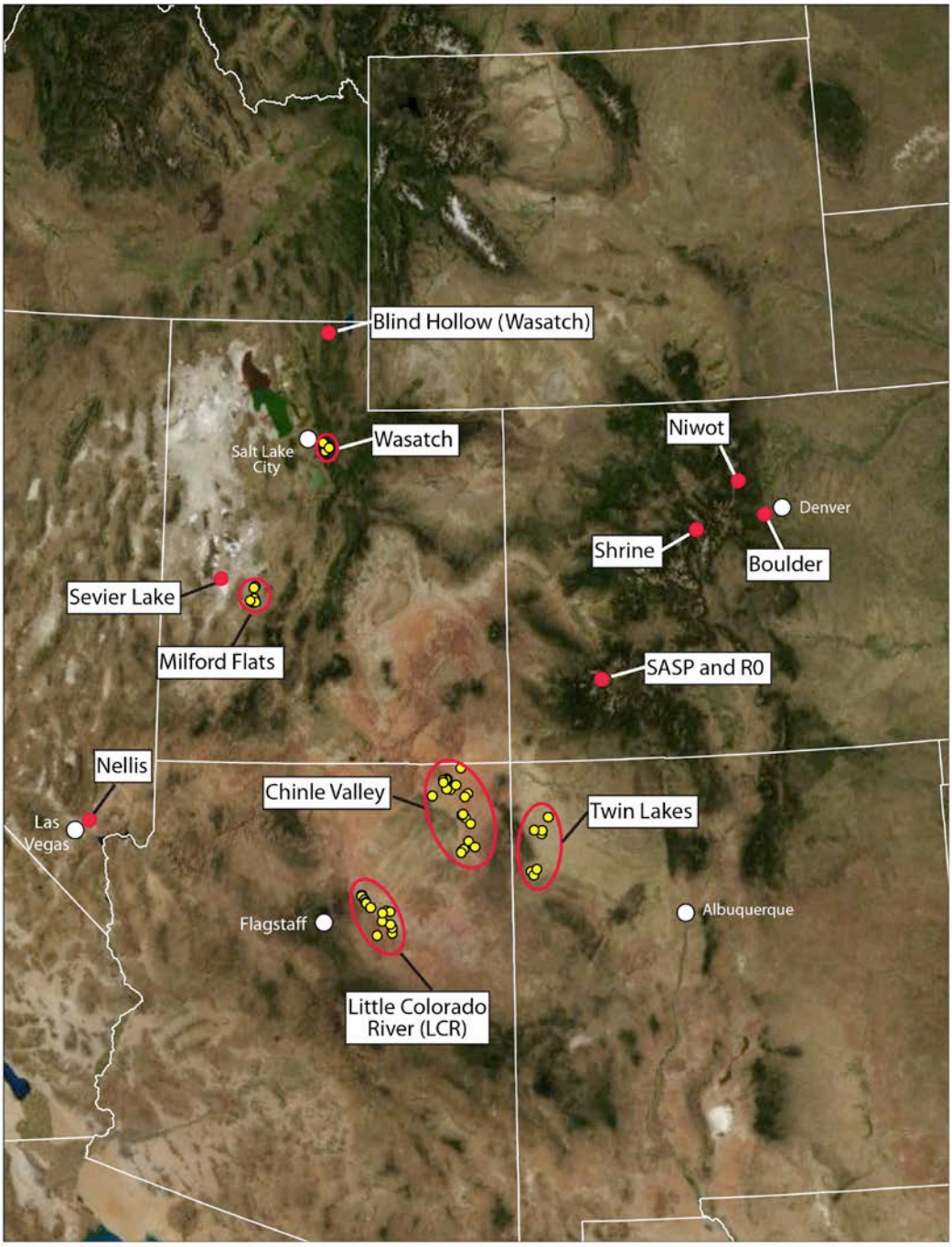

Figure 2-1: American southwest dust collection sites. Wasatch locations and sites in Colorado were collected from snow pack (DOS) while Chinle Valley, Twin Lakes, Little Colorado River, Nellis, Milford Flats, and Sevier Lake were sediment source areas (DSA).

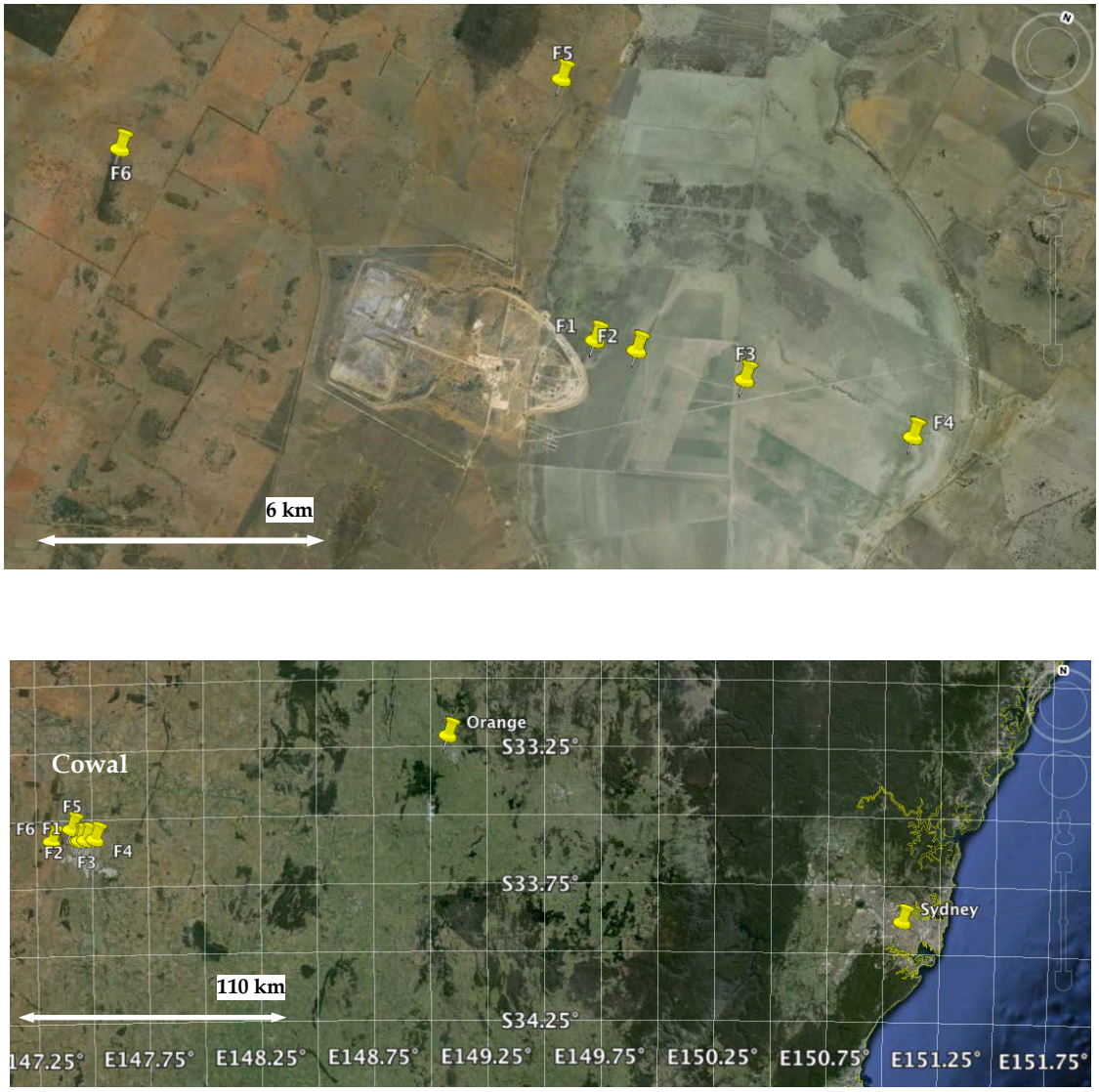

Figure 2-2: Red Dawn Sampling Locations. Top shows sites F1-F6 of the Lake Eyre Basin, NSW, Australia. Bottom is smaller scale showing Lake Cowal to Sydney with Orange location in between.

2.2 *Sample Preparation:*

To prepare magnetic measurements, gelatin capsules were filled with 100-200 mg of collected atmospheric dust or surface sediment and weighed in order to mass normalize magnetic measurements. Quartz "Fiberfax" wool was placed in the top of each capsule to hold the contents in place. Capsules were then sealed with Kapton tape and placed into plastic straw holders. Remanence measurements were carried out on the capsules in small segments of straw contained in plastic boxes in order to preserve orientations in three dimensions. Mössbauer samples were prepared separately in standard plastic holders sealed with Kapton Tape.

2.3 *ARM Measurements*

Anhysteretic remanent magnetization (ARM) is produced by the dual actions of an alternating field and a small DC biasing field. By applying a biasing field along with the AC demagnetizing field, an asymmetry is created in the demagnetization process, resulting in a small magnetic moment. Grains that acquire ARM are those with coercivities in the range of the AC demagnetizing field. In magnetite, ARM affects the 0.05 to ~10 um size range of SD grains (REF). Hematite and goethite grains generally have coercivities higher than the

fields used in this study and so do not carry ARM. Coercivity is dependent, however on grain size so very coarse hematite could acquire ARM.

ARM was imparted as follows. The samples were first demagnetized in all directions to the maximum AC field of 200 mT in a DTech alternating field (AF) demagnetizer and measured in a 2G Enterprises U-channel magnetometer in the x, y, and z directions (arbitrarily chosen with the long axis of the gelatin capsule in the z direction). This step defines a baseline, demagnetized level. ARM was acquired in an alternating field of 120 mT with a 100 uT biasing field along the z axis. The ARM value was found by taking the difference in magnetization between the two steps and dividing by sample mass to get units of Am^2/kg.

2.4 Hysteresis Properties

Hysteresis loops were measured on a Princeton Applied Research Vibrating Sample Magnetometer (VSM). Each sample was measured at room temperature on a VSM from +1 T to -1 T and back in 2.5 mT increments at a sensitivity level on the order of 2-50 uAm^2/kg, creating a hysteresis loop that gives properties of the sample such as saturation of remanence (Mr), saturation magnetization (Ms), and coercivity (Br). Such parameters were calculated using programs developed by the Institute for Rock Magnetism. Samples were then

given a saturating field of 1 T and progressively demagnetized in a backward field that step-wise increased in magnitude on a log scale to -1 T in order to determine coercivity of remanence (Bcr). The ratio of these four properties indicates overall grain size.

2.5 HIRM Measurements

Hard isothermal remanent magnetization (HIRM) separates low coercivity magnetization (soft) from high coercivity (hard). Fields can be applied to samples using a pulse magnetometer or by setting a field on a VSM. By giving a sample a strong induced magnetization in one direction and a weak field in the reverse, samples will have high and low coercivity fractions magnetized in opposite directions, which can then be measured and calculated. The low coercivity fraction correlates to the strongly magnetic magnetite and oxidized maghemite while the high coercivity fraction correlates to hematite and possibly small amounts of goethite.

This study calculated HIRM by running each sample through a tray in a VSM at room temperature so that the gel capsules were oriented with their long axes in the direction of the 1000 mT field. Remanence was measured on a u-channel magnetometer in the X, Y, and Z directions. The process was then repeated but with the samples oriented in the VSM backwards under a 300 mT

field. Additionally, HIRM was automatically calculated by the VSM on backfield measurements, giving two separate results. HIRM values were then calculated as follows:

$$HIRM = (IRM_{-300} + IRM_{1T})/2$$

Liu et. al., 2007 created a new parameter to support the validity of HIRM measurements. Their study found that substantial Al substitution in hematite and goethite affects coercivities and therefore influences the absolute and relative abundances of hematite and goethite found by HIRM parameters. They introduce an "L-ratio" that, if constant, can reinforce HIRM results. Fluctuations in the L-ratio instead indicate that coercivities may be varying due to changes in mineral composition. The L-ratio is defined as:

$$\text{L-ratio} = IRM_{AF@300mT} / IRM_{AF@100mT}$$

The measurement only requires applying a 1 T IRM followed by a 100 mT and then a 300 mT AF demagnetization. The instruments used in the L-ratio are flexible and can be measured instead on the VSM using the same steps as HIRM measurements with an added 100 mT backfield step. The L-ratio is then substituted as:

$$\text{L-ratio} = HIRM/[0.5 * (SIRM + IRM_{-100mT})]$$

2.6 Low Temperature Measurements

Low temperature remanence was measured on a Quantum Design Magnetic Property Measurement System (MPMS). The amount of remanence carried by a sample varies by temperature and field so samples were measured on warming and cooling in DC fields to examine the effects on magnetic moment, particularly mineral phase transitions at known temperatures. In the first temperature cycle, samples were cooled down to 10 K in a 2.5 T field (field cooled) and measured on warming without a field. The remanence was compared to cooling the sample in zero-field and giving it an induced magnetization at 10 K before measuring on warming without a field (zero-field cooled). Finally, samples were measured once again on cooling and warming after being given an IRM in 2.5 T at room temperature.

The MPMS was also used to measure changes in susceptibility with temperature in AC fields at five frequencies between 1 and 1000 Hz in order to discern the frequency dependence and viscosity of the magnetic grains over a range of temperatures (20 K to 300K). As the AC field varied sinusoidally, magnetic grains responded instantaneously producing the in-phase susceptibility (X′) while other grains responded sluggishly, becoming out-of-phase with the alternating current (X″). While there can be other causes for x″

such as domain wall relaxation in coarse grained magnetite and titanomagnetite below 100 K, time-dependence is often related to SP grain size.

2.7 Goethite tests

Standard FC-ZFC measurements are useful for determining phase transitions in minerals but are not advantageous when characterizing goethite because there are no transitions associated with this mineral. Furthermore, magnetite overwhelms the magnetic signal of weaker minerals such as goethite. Three tailored goethite tests were designed in order to examine behavior at fields past the hematite saturation limit and on heating through the goethite Curie temperature (393 K), thereby thermally demagnetizing the goethite fraction alone. In one test, AF demagnetization was implemented in order to prevent low coercivity magnetite from overwhelming the goethite and hematite signals. In this way, a more thorough evaluation of the goethite fraction can be made.

2.7.1 Maher Test

The Maher Test is based on the Maher et. al. (2004) method in which they utilized goethite's high coercivity to measure the difference between magnetic moments at high fields (1-2 T) and very high fields (5-7 T). The current study, limited to 5 T, measured remanence on cooling to 10 K after exposure to 2 T and

5 T fields at room temperature (Figure 2-3). The difference in the moments between points 1 (5T) and 2 (2T) were calculated as a percent increase in remanence due to goethite. The same percent increase was calculated again at 10 K between points 3 and 4. Because goethite has no low temperature transitions, and remanence increases monotonically with decreasing temperature (Dekkers, 1989; France and Oldfield, 2000), slope was calculated from points 1 and 3 at 5 T and from points 2 and 4 at 2 T to gauge the change at high fields.

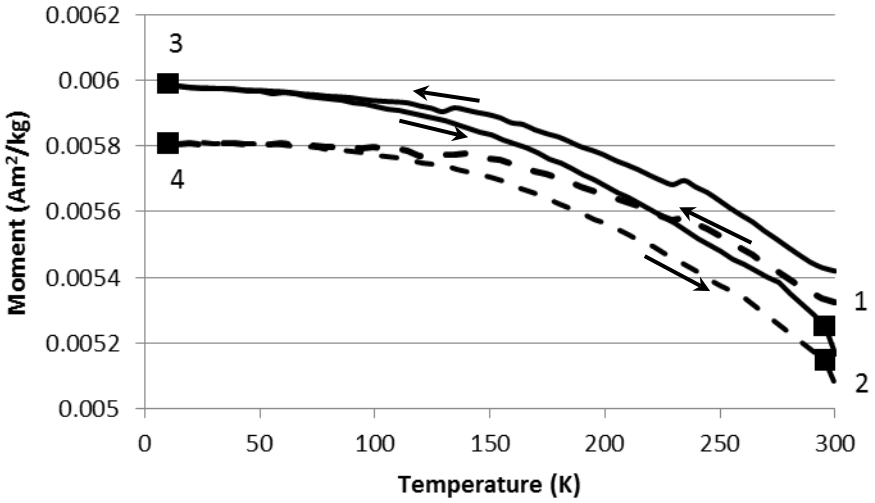

Figure 2-3: Maher Test. Dashed lines represent moment after exposure to a 2 T field. Solid lines represent moment after exposure to a 5 T field. Difference in magnetization was calculated by subtracting points 2 from 1 and 4 from 3. Slopes at each field strength were calculated between points 1 and 3 (5T) and points 2 and 4 (2T).

2.7.2 Guyodo Test

In order to isolate the magnetic signal of goethite, Cater-Stigliz et. al., 2006 and Guyodo et. al., 2006 used high fields and thermal demagnetization of goethite to measure changes in magnetic moment. This version of the goethite test was adapted by this study to measure and compare amounts of magnetite, hematite and goethite in atmospheric dust. Using straw holders in the MPMS, each sample was cooled in a 2.5 T field from 400 to 300 K to thermally magnetize all the goethite while also saturating the magnetite and the majority of the hematite. The field was then reduced to zero and the samples were cooled to 20 K and warmed back to room temperature. The sample was then removed from the MPMS and was partially AF demagnetized on the DTech AF demagnetizer at 200 mT in order to remove the low coercivity fraction, which would provide a stronger signal of the high coercivity components, goethite and hematite. After partial demagnetization, the sample was returned to the MPMS and once again measured on cooling and warming before it was heated to 400 K, thermally demagnetizing the goethite above T_C. The remanence of the sample dropped on warming by the amount contributed by goethite. The final step was another cooling and warming measurement of the remaining magnetization, which would correspond to any other high coercivity components, mainly hematite. Figure 2-4 shows a diagram of the Guyodo goethite test. Magnetite calculations were made by taking the difference in remanence at 300 K before and after AF

demagnetization. The goethite contribution is the difference in remanence at 300 K before and after thermal demagnetization. The remaining magnetization at 300K after cooling and warming at the end was the amount of remanence attributed to hematite.

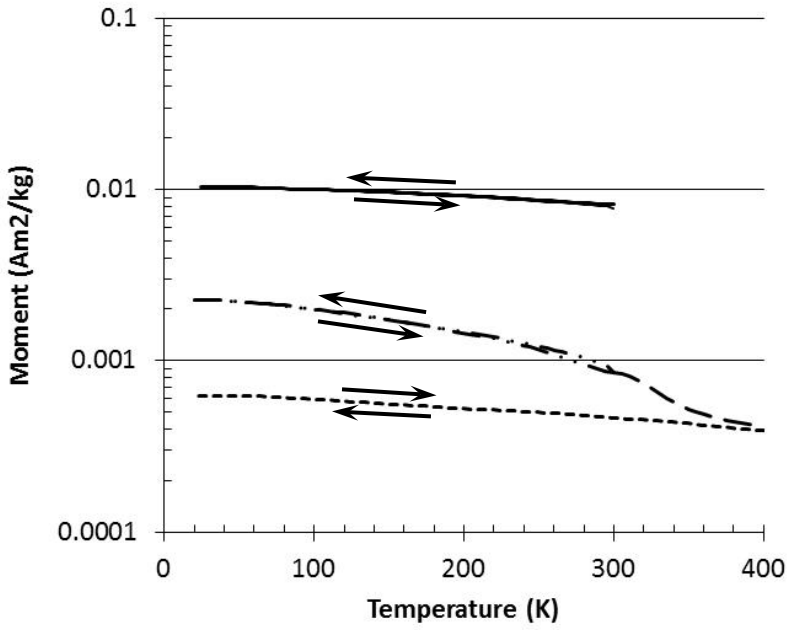

Figure 2-4: Remanent magnetization behavior for the Guyodo Test on Australian sample Orange. Solid lines represents moment on cooling and warmng after application of 2.5 T field cooled through 400 K. Dot-dash line is moment after AF demagnetization to 200 mT. Long dash shows thermal demagnetization of goethite. Short dashes are moment due to high-coercivity minerals such as hematite. Measurement made with the field on is not shown for scaling purposes.

2.7.3 Guyodo-Lascu Test

Lascu and Feinberg (2011) made similar measurements using only the thermal demagnetization step so that samples did not have to be removed from the MPMS by the user. Without the AF demagnetization step, magnetite would overpower the signal; therefore a smaller 10 mT IRM was applied by this study in order to prevent the saturation of magnetite grains. Eleven samples were measured using this alternate method in order to compare the goethite signal and weigh the attributes of each method. These samples were cooled through the Curie temperature from 400 to 300 K in a 10 mT field and measured on cooling to 20 K and back to room temperature with the field off. Instead of being AF demagnetized, samples were immediately heated to 400 K for thermal demagnetization and were once more measured on cooling and warming. See Figure 2-5 for a diagram of the Guyodo-Lascu test.

To provide additional information about grains that remained unblocked at room temperature, the whole process was repeated a second time but with an initial field applied longer from 400 K to 200 K in order to magnetize a greater fraction of particles. Five points along the warming and cooling curves, marked on the figure below, were used to calculate iron oxide mineral percentages. The differences between points 1 and 2 at 300 K and 3 and 4 at 200 K before and after thermal demagnetization show how much of the magnetic signature is due to

goethite. The difference in moment between points 3 and 5 at 200 K is due to grains that have blocking temperatures between 200 and 300 K.

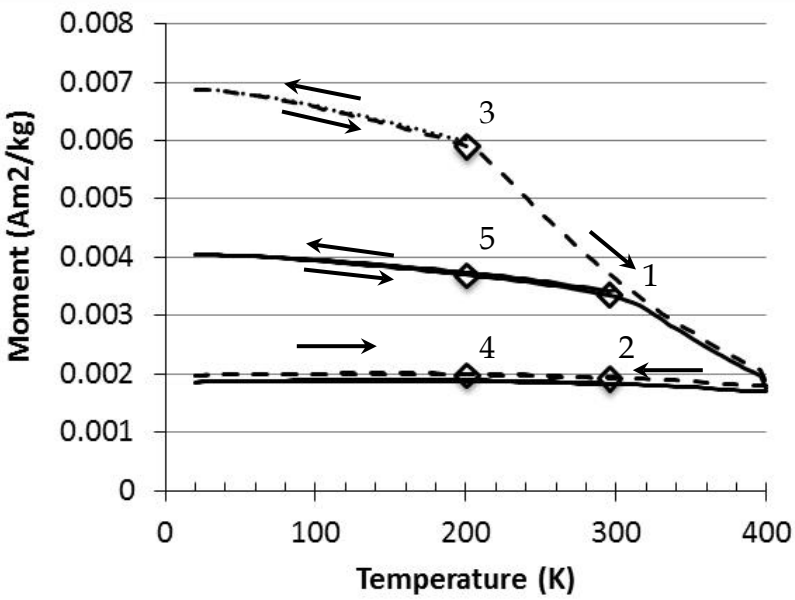

Figure 2-5: Guyodo-Lascu Test. Solid lines represent measurements made after cooling through 400 K to room temperature. Dashed lines show measurements made after cooling through 400 K to 200 K. Measurements made while cooling with the field on are not shown.

2.8 Coercivity Unmixing

The minerals that contribute magnetic properties to a sample have different coercivities that together blend into the magnetic signature. By fitting demagnetization curves to a model and taking the derivative, each coercivity contribution can be isolated. The resultant curve can then be fit to individual components to determine the coercivity and percent of remanence each contributes.

In preparation for the coercivity unmixing, the average of three to five backfield curves (depending on noise levels) up to 1.5 T was used as input for the program MagMix, written by Ramon Egli (2004). Fitting was done according to the program to get an output for each magnetic component defined by its amplitude, coercivity, dispersion, and skewness.

2.9 Mössbauer Spectroscopy

Samples were measured using Mössbauer spectroscopy at both room temperature and 4.2 K to characterize iron-oxide mineralogy. A ^{57}CO/Rh source was used with a conventional constant-acceleration spectrometer in transmission geometry. An alpha-Fe foil was used at room temperature to calibrate isomer shifts and velocity scale. Each sample was run for 1-3 days to obtain good counting statistics. Mossbauer spectra, consisting of sextets and doublets, were fit using the NORMOS program (Brand, 1987). The spectral fits provide estimates for the isomer shift (IS), hyperfine field (B_{hf}), and quadrupole splitting (QS) parameters for each subspectra. The final fittings of Mossbauer spectra to obtain IS, QS, and B_{hf} magnitudes were carried out by Dr. Thelma Berquó. Because of the complexity of multiple components, the number of components was limited to three to five. Several unknown paramagnetic doublet components were not identified in the fitting process. This was because it could

not be determined which of several minerals was a better fit. These components are simply listed as percentages of the Fe^{2+} or Fe^{3+} they contribute.

2.10 High Field Acquisition

A recent re-fitting of an electromagnetic pulse magnetizer with a high-field coil made it possible to impart magnetic fields as high as 9.2 T. Samples are magnetized in straw holders and so may be used in conjunction with all other instruments. The field is set by applying a known voltage, which linearly corresponds to magnetic fields in mT with a coefficient of 0.0246, meaning that one volt changes the field by 24.6 mT. The accuracy of the pulser is +/- 0.5 volts, which corresponds to an error of 12.3 mT in either direction.

IRM acquisition curves were measured on synthetic hematite and goethite samples WS222, Nano Goethite 10x100, Skyspring hematite, and Nano hematite 25nm. In the purest samples, hematite was saturated by 2.5 T while nanogoethite had only just begun to acquire remanence. Fields of 1, 3, and 9 T were chosen as crucial acquisition points, between which remanence of hematite and goethite were acquired. The gain in remanence between one and three tesla is attributed to hematite and goethite while remanence gained in higher fields is due to goethite alone. Backfields of 300 mT could then be applied to separate the soft magnetite component.

Natural samples were measured at these intervals to determine contributions from each mineral. Parameters from Maher et. al. (2004) were adapted to the fields used in this study. Her study used very high field HIRM at 2 and 7 tesla to calculate the parameter H%. Substituting the field strengths, this study defined H% as:

$$H\% = (HIRM_{9\text{-}3T}/HIRM_{3\text{-}1T}) * 100$$

This parameter gives the proportion of remanence gained above 3 T as a percentage of total IRM acquisition and represents the amount of goethite contribution.

3 Results

The following are results from the magnetic measurements used to determine iron oxide properties and contributions.

3.1 ARM Results

The results of ARM measurements are shown in Figure 3-1. xARM takes the effect of the field strength out of the ARM measurement. Values have been field normalized and averaged by location. Bodele dust was not measured.

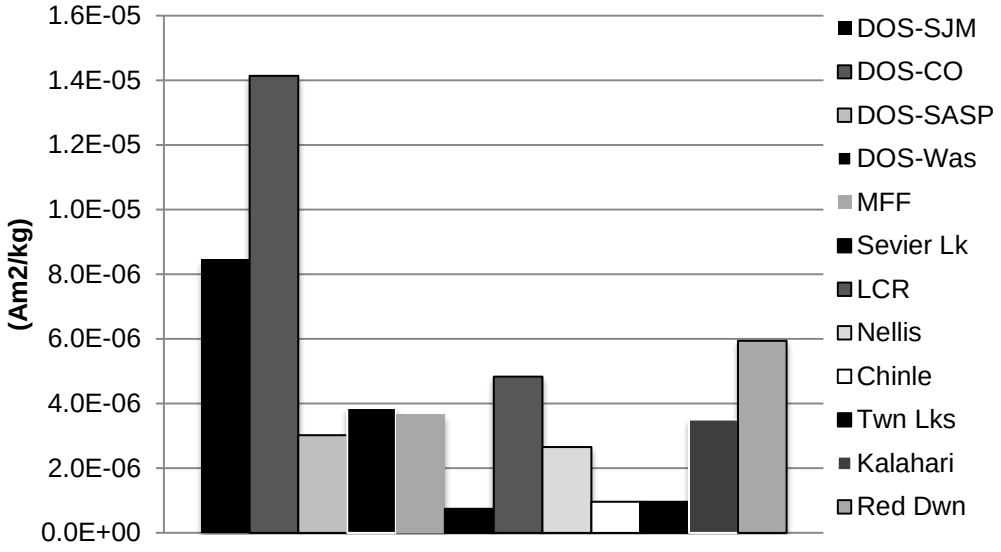

Figure 3-1: XARM averages by location.

3.2 Hysteresis Properties Results

Hysteresis properties provide grain size information about mostly the ferromagnetic contribution of magnetic minerals, magnetite and maghemite. Room temperature hysteresis loops show varying degrees of saturation due to high coercivity minerals. All loops have a prominent paramagnetic contribution. Hysteresis properties for all samples are summarized in the appendix. Table 3-1 below shows averages by location. Coercivities range from 1.08 mT (Bodele) to 20.76 mT (Tucker Flat-LCR). Coercivity of remanence ranges from 13.67 mT (NN110314-2-Chinle) to 61.51 mT (Tucker Flat-LCR). Both Bc and Bcr were often much higher for synthetic samples of nano hematite (ex. 130.39 mT) and nano goethite (164.52 mT). Saturation magnetization ranges from 0.0022 to 0.5196 Am^2/kg, with both end values from the Bodele area. Highest averaged values, however, were from MFF and Wasatch DOS samples (Figure 3-2). Lowest averaged values lowest were from Nevada (Nellis) and Arizona (Chinle Valley and Little Colorado River).

The hysteresis loop shape parameter, sigma, (described in Fabian, 2003) compares the area in the hysteresis loop to an ideally symmetrical loop. Sigma values were mostly near zero, indicating symmetry. Some values were higher such as those of Chinle Valley and LCR, approaching one half. The only negative sigma values from in the American southwest samples were from MFF, Sevier Lake, and Wasatch DOS.

Table 3-1: Hysteresis Properties

Sample Location	Ms (Am^2/kg)	Mr (Am^2/kg)	Bc (mT)	Bcr (mT)
DOS-Boulder	0.0730	0.0070	9.3433	38.7467
DOS-R0	0.0941	0.0124	12.0790	38.4764
DOS-SASP	0.0565	0.0085	11.1315	33.3712
DOS-Wasatch	0.1410	0.0166	8.9283	25.1695
MFF	0.1322	0.0147	8.8945	27.9565
Sevier Lake	0.0389	0.0040	7.3818	27.6566
LCR	0.0352	0.0089	15.8329	40.9102
Nellis	0.0229	0.0041	12.1899	35.8170
Chinle Valley	0.0241	0.0040	11.5921	33.4098
Twin Lakes	0.0561	0.0048	6.1297	32.3388
Kalahari	0.0760	0.0171	15.4413	36.2200
Lake Cowal	0.0183	0.0039	13.5556	32.8399
Orange	0.0521	0.0104	7.0188	18.2603
Sydney	0.2124	0.0216	7.6675	25.8989
Bodele	0.0511	0.0094	10.7308	32.6943

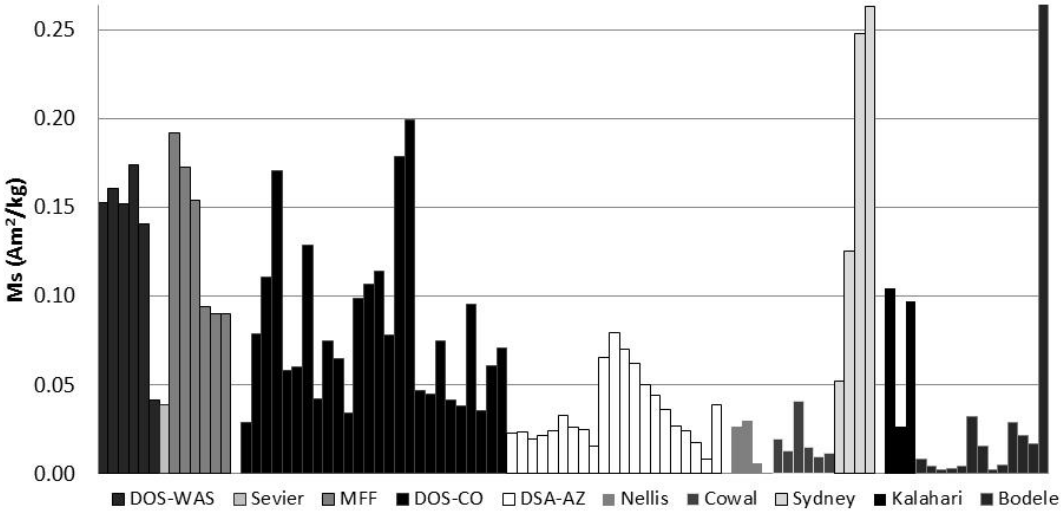

Figure 3-2: Saturation magnetization (Ms) by location. DOS is shown next to proposed DSA. Also shown are African and Red Dawn samples sorted by location. Note that the strongest Bodele sample goes off the chart to 0.52 Am²/kg.

3.3 HIRM Results

Table 3-2 below summarizes the HIRM results averaged by location. S300 is the remanence from the magnetically soft, low coercivity components like magnetite and maghemite. HIRM is listed by machine on which measurements were carried out and represents the remanence of magnetically hard, high coercivity minerals like hematite and possibly goethite. There is disagreement between the two machines. SIRM is the total magnetization after a 1 T IRM and represents primarily the ferrimagnetic components.

Table 3-2: HIRM Results

Sample Location	S300 (Am^2/kg)	$HIRM_{VSM}$ (Am^2/kg)	SIRM (Am^2/kg)	$HIRM_{UC}$ (Am^2/kg)
DOS-Boulder	0.8844	-	6.876E-03	4.138E-04
DOS-R0	0.9122	6.609E-04	1.173E-02	4.953E-04
DOS-SASP	0.8716	4.658E-04	7.738E-03	4.832E-04
DOS-Wasatch	0.9691	1.710E-04	1.493E-02	2.369E-04
MFF	0.9131	3.146E-04	1.423E-02	4.321E-04
Sevier Lake	0.9415	3.838E-05	3.789E-03	1.109E-04
LCR	0.7647	8.513E-04	8.865E-03	9.496E-04
Nellis	0.8949	1.946E-04	4.099E-03	1.946E-04
Chinle Valley	0.7123	3.696E-04	3.959E-03	6.151E-04
Twin Lakes	0.8534	2.167E-04	4.355E-03	3.134E-04
Kalahari	0.8239	6.686E-04	1.605E-02	1.271E-03
Lake Cowal	0.7883	4.067E-04	4.114E-03	3.076E-04
Orange	0.8959	5.223E-04	9.395E-03	3.296E-04
Sydney	0.9602	3.455E-04	2.269E-02	4.621E-04
Bodele	0.8683	2.536E-04	-	-

3.4 Susceptibility

Table 3-3, below, shows the average in-phase susceptibility at 1 and 1000 Hz along with out-of-phase susceptibility (X"), ferrimagnetic susceptibility (Xf) and frequency dependence (Xfd%) by location. The entire table can be found in the appendix. Xf is the susceptibility contribution of the ferrimagnetic component while Xhf is the susceptibility from the high field component with

the ferrimagnetic signal subtracted out. Xfd% shows the relative abundance of SP grains. Highest Xfd% was measured from LCR, AZ and Australian dust. Samples with lowest Xfd% were found in Sevier Lake and Milford Fire Flats.

Table 3-3: Susceptibility

Sample Location	X′ 1Hz	X′ 1000 Hz	X″ 1 Hz	Xf	Xhf	Xfd%
DOS-Boulder	7.43E-07	7.01E-07	8.94E-09	7.15E-07	2.84E-08	2.37%
DOS-R0	8.69E-07	8.39E-07	1.29E-08	8.36E-07	3.35E-08	2.20%
DOS-SASP	5.85E-07	4.79E-07	9.99E-09	5.41E-07	4.34E-08	2.75%
DOS-Was	1.29E-06	1.24E-06	1.50E-08	1.24E-06	4.98E-08	2.01%
MFF	1.20E-06	1.16E-06	1.32E-08	1.16E-06	4.48E-08	1.42%
Sevier Lake	2.88E-07	2.81E-07	2.37E-09	2.78E-07	1.06E-08	0.90%
LCR	5.01E-07	4.37E-07	1.45E-08	4.32E-07	6.92E-08	4.43%
Nellis	3.37E-07	3.02E-07	8.25E-09	2.80E-07	5.71E-08	3.89%
Chinle Valley	2.48E-07	2.54E-07	4.34E-09	2.04E-07	4.43E-08	2.77%
Twin Lakes	5.13E-07	5.13E-07	7.78E-09	4.62E-07	5.09E-08	1.47%
Kalahari	6.16E-07	8.56E-07	1.77E-08	5.56E-07	5.98E-08	4.86%
Lake Cowal	3.60E-07	6.37E-07	1.67E-08	2.90E-07	7.02E-08	7.21%
Orange	2.05E-06	1.48E-06	1.34E-07	1.95E-06	1.02E-07	9.89%
Sydney	2.40E-06	1.60E-06	7.26E-08	2.33E-06	7.56E-08	4.17%
Bodele	5.66E-07	5.35E-07	8.35E-09	5.01E-07	6.48E-08	3.92%

3.5 Mössbauer Spectroscopy Results

Mössbauer spectroscopy was performed on 16 samples. None had enough magnetite to be detected by this method. Table 3-4 shows the percentage of hematite and goethite at both room temperature and 4.2 K. A third column for hematite lists the increase in mineral percentages at low temperature. See the appendix for percentages of the paramagnetic iron content.

Table 3-4: Mössbauer Spectroscopy Results

Sample	% Ht 300 K	% Ht 4.2 K	Incr. (%)	% Gt 300 K	% Gt 4.2 K
R08E1	30			0	
Niwot Ridge	37			0	
Blind Hollow	17	17	0	0	18
Lower Mill B				0	
L Red Pine	20	13*	-7	0	21
09296	16	16	0	0	16
10470	8.54	-		0	
Dinnebito	20.8	21	0.2	0	18
Mud Lk up. s.	50	50	0	0	12
Toolani Lk W	18	18	0	0	0
Rd6732 Pl N	26	26	0	0	0
Tucker Flat 3	36	36	0	0	0
Nellis 3.2	13.00				
Stop 23 TPW	24.6				
NN110314-2	35.1				
NN110316-2	5.7				

3.6 Goethite Tests Results

3.6.1 Maher Test

The Maher test did not take any mineral other than goethite into account. All samples did show an increase in remanence between 2 and 5 T that would only be attributed to goethite. Table 3-5 shows the change in slope on warming at both field strengths and the percent increase in moment attributed to goethite.

Table 3-5: Maher Test Results

Sample	Location	Slope 2 T	Slope 5T	% Gt 300K	% Gt 10K
Dinnebito	LCR	-2.32E-06	-2.59E-06	2.03	3.50
Mud Lk Upper Loose	LCR	-4.33E-06	-4.54E-06	1.76	2.11
Stop 15	Chinle	-6.88E-07	-9.84E-07	3.58	9.11
NN110314-6	Chinle	-3.83E-06	-4.27E-06	7.38	9.81
09296	MFF	-8.97E-07	-9.95E-07	3.49	3.89
Nellis 2.2	Nellis	-5.39E-07	-7.00E-07	2.51	8.56
Nellis 3.2	Nellis	-2.03E-06	-2.50E-06	2.80	5.62
Orange	Australia	-5.84E-06	-7.19E-06	3.15	8.72
GB-1	Kalahari	-9.41E-06	-1.04E-05	2.70	9.65
Nanohematite	25 nm	4.07E-05	4.26E-05	4.19	2.05
Alpha Fe_20_3	Skyspring	1.43E-04	1.43E-04	9.42	9.29
Gamma Fe_20_3	Skyspring	-1.10E-03	-1.28E-03	2.14	2.74
Nanogoethite	10x100 nm	-2.47E-06	-1.57E-05	499.42	1031.63

3.6.2 Guyodo Test

The Guyodo test provided remanence magnetization between each step corresponding to low coercivity magnetite, high coercivity hematite, and goethite mineral contributions. The remanence of each was divided by the total magnetization to get a percent contribution. Table 3-6 lists values of representative samples. A full list of the measured moments and percent of total magnetization to which the minerals correspond can be found in the appendix.

Table 3-6: Guyodo Test Results

Sample	Location	Mgt [Am²/kg]	Ht [Am²/kg]	Gt [Am²/kg]	Mgt %	Ht %	Gt %
SASP D4	DOS-SASP	4.49E-03	6.95E-04	1.06E-04	84.86	13.14	2.00
Wasatch 09	DOS-Was	1.32E-02	5.84E-04	1.02E-04	95.08	4.19	0.73
09296	MFF	7.69E-03	6.35E-04	5.11E-05	91.80	7.59	0.61
Dinnebito	LCR	4.54E-03	9.09E-04	1.39E-04	81.23	16.27	2.49
Mud Lk. Up.	LCR	1.51E-02	2.37E-03	4.20E-04	84.45	13.21	2.34
Tucker Flat 3	LCR	4.39E-03	1.59E-03	2.94E-04	69.92	25.39	4.69
Nellis 2.2	Nellis	7.03E-04	6.34E-05	2.33E-05	89.02	8.03	2.95
Nellis 3.2	Nellis	4.47E-03	5.09E-04	1.72E-04	86.76	9.89	3.35
Stop 15 TC	Chinle	1.44E-03	2.25E-04	6.86E-05	83.06	12.98	3.96
NN110314-6	Chinle	4.14E-03	1.85E-03	1.44E-04	67.47	30.18	2.35
Orange	Australia	7.36E-03	4.66E-04	3.85E-04	89.63	5.68	4.69
GB1	Kalahari	3.79E-03	7.95E-04	1.32E-04	80.37	16.84	2.79
Nano Gt	10x100	2.00E-03	1.26E-05	2.04E-02	8.90	0.06	91.05
Nano Ht	25 nm	1.71E-02	3.15E-02	7.22E-03	30.62	56.45	12.93
Alpha Fe_2O_3	Skyspring	3.98E-02	2.92E-02	2.68E-02	41.55	30.5	27.95

3.6.3 Guyodo-Lascu Test

Table 3-7 lists the values from the Guyodo-Lascu test. It includes the percentage of the remanence lost on thermal demagnetization of goethite after field cooling to 300 K and 200 K. The final column shows the percent increase in remanence due to grains with blocking temperatures between 200 and 300 K. In other words, Dinnebito had a moment 35.61% higher when cooled in a field to 200 K than when cooled to 300 K. Grains on the SP/SD boundary provided the increase in remanence.

Table 3-7: Guyodo-Lascu Test Results

Sample	Location	% Gt 300K	% Gt 200K	% Gt SP/SD
Dinnebito	LCR	44.95	63.24	35.61
Mud Lk Upper Loose	LCR	46.80	61.71	31.40
Stop 15	Chinle	51.25	74.45	47.38
NN110314-6	Chinle	45.09	66.37	35.01
09296	MFF	39.78	46.61	16.53
Nellis 2.2	Nellis	48.55	74.99	48.55
Nellis 3.2	Nellis	47.61	64.92	33.23
Orange	Australia	45.46	66.40	37.34
GB-1	Kalahari	57.03	77.81	40.38
Nanohematite	25 nm	32.11	34.26	6.24
Alpha Fe_2O_3	Skyspring	75.78	76.78	10.91
Nanogoethite	10x100 nm	97.47	98.28	6.72

3.7 Coercivity Unmixing Results

Figure 3-3 below shows component distributions for samples F1-F4 and F5-F6 overlaid on the same graph. The axis along the bottom shows the log of coercivity and the vertical axis displays amplitude or percent contribution of each component. Some amplitudes exceed 100 percent due to the way the program calculates high coercivity components. In the following table, amplitudes have been scaled down to 100%. Table 3-8 summarizes all the components for Australian sites F1-F6. These results were the most extensively measured and represent changes in composition down the wind stream.

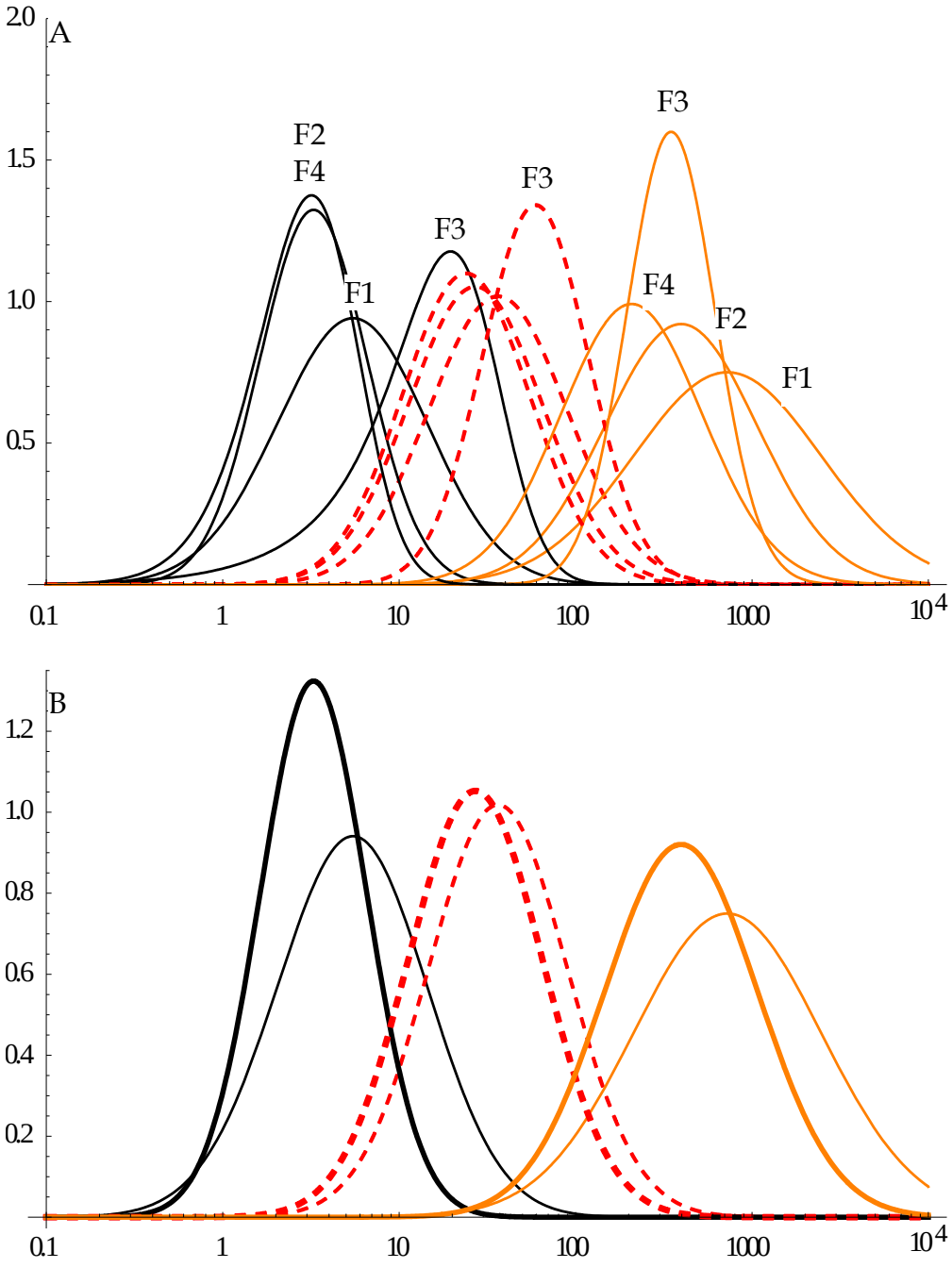

Figure 3-3: Coercivity Unmixing. A) Components of sites F1-F4. Middle component appears in dashed lines. B) Components of sites F5 and F6 (bold). Middle components dashed.

Table 3-8: Australia Components

Sample	Comp 1				Comp 2				Comp 3			
	A	MDF	S	Q	A	MDF	S	Q	A	MDF	S	Q
F1	8.7	0.727	0.425	0.869	61.7	1.573	0.392	1.000	29.6	2.863	0.536	1.000
F2	5.9	0.515	0.301	1.000	76.3	1.432	0.379	1.000	17.9	2.598	0.433	1.000
F3	79.3	1.270	0.425	0.566	13.2	1.925	0.226	1.000	7.4	2.514	0.249	1.000
F4	11.7	0.691	0.381	1.000	71.9	1.412	0.354	-0.772	16.5	2.296	0.388	1.000
F5	7.7	0.555	0.389	0.686	64.9	1.453	0.370	-0.840	27.4	2.619	0.507	1.000
F6	51.2	1.252	0.453	0.568	27.6	1.837	0.320	1.000	21.1	2.805	0.548	1.000

Table of components for sites F1-F6 with parameters for amplitude (A), median destructive field (MDF) in log scale, Dispersion Parameter (S), and Skewness (Q). Squarness remained unadjusted for all samples and was not included.

3.8 Temperature Dependence

Many of the low temperature transitions measured in the Guyodo goethite test were suppressed in the natural samples. Transition suppression is not uncommon in very fine grained particles. Synthetic standards, the 25nm hematite for instance, would have suppressed Morin transitions as low as 150 K, over 100 degrees lower than expected. Many samples also showed temperature hysteresis in which the transition temperature was higher on warming than on cooling. Table 3-9 lists several representative samples and their transition temperatures based on derivative curves averaged from FC, ZFC, RTSIRM, and goethite tests. T_V and T_M on warming were averaged from FC, ZFC, and RTSIRM curves on warming. Low temperature transitions on cooling come from averages of cooling curves from RTSIRM and goethite tests.

Included also is the goethite Curie temperature measured on cooling in a 2.5 T field during the thermal magnetization step of the goethite test and the blocking temperature of goethite in zero field shown by a sudden drop in remanence on warming to 400 K. Remanence is measured in 5 K increments, so error can be as much as 2.5 K. Transition temperatures were not found in every measurement, for instance, when individual mineral remanence was weak either because the remanence was obscured by stronger magnetic signals or because the mineral was not present.

Table 3-9: Temperature Dependence

Sample	T_V Cooling	T_V Warming	T_M Cooling	T_M Warming	T_C Cooling	T_B Warming
SASP D4	121	118	232	-	357	322
Wasatch Bulk	119	112	257	257	356	-
09296	115	121	263	267	352	317
Tucker Flat 3	119	123	226	-	352	313
Nellis 2.2	122	-	251	-	361	-
NN110314-6	112	125	246	-	362	-
F1	118	123	232	278*	356	313
BK1	121	124	250	-	348	313
Nano Gt 10x100	-	-	258	-	372	352

*The Morin transition for sample F1 on warming was based on the derivative of the RTSIRM warming curve and is higher than would be possible for hematite.

3.9 High Field Acquisition

The samples from the Bodele depression in northern Sahara Desert were measured up to 9 T. Table 3-10 shows the magnetization gained between each acquisition step and the percent increase in moment from 3 to 9 T, which indicates percentage of remanence gained above the hematite saturation. The H% value is a portion of the remanence attribute to goethite alone. Only samples that had positive H% values are significant. Negative values are due to possible machine error. A synthetic goethite standard and one sample from Orange, Australia are included for comparison.

Table 3-10: High Field Acquisition Results

Sample	Size	HIRM $_{9\text{-}3\ T}$	HIRM $_{3\text{-}1\ T}$	H%
CH 11	125-2000 um	5.71E-05	2.29E-04	**24.91**
CH 11	63 um	1.27E-04	1.03E-03	**12.28**
CH 23	63 um	2.83E-05	9.03E-05	**31.40**
CH 24	63 um	-9.12E-05	3.42E-05	-267.05
CH 2	63 um	-1.59E-03	1.41E-03	-112.90
CH 39	63 um	-4.46E-02	5.94E-03	-750.71
CH 62	63 um	-2.36E-04	7.81E-05	-302.37
CH 80	125-2000 um	-2.46E-04	2.47E-05	-995.41
CH 80	63 um	-4.02E-05	1.54E-03	-2.61
CH 81	125-2000 um	-5.75E-05	6.58E-05	-87.38
CH 81	63 um	3.15E-04	1.15E-03	**27.34**
CH 8	125-2000 um	3.40E-06	4.22E-05	**8.05**
CH 8	125-2000 um	3.93E-05	1.57E-04	**25.06**
CH 8	63 um	5.87E-04	1.06E-03	**55.59**
Orange	Australia	-8.20E-05	8.24E-04	-9.95
NanoGt	10x100 nm	1.03E-05	4.85E-07	**2121.74**

4 Discussion

4.1 Composition

The American southwest dust shows ubiquitous presence of magnetite but in very small fractions of a weight percent. The magnetite grain size is too large to be biogenic in origin and is likely weathered from surrounding igneous rocks.

Australian dust samples all contain small amounts of magnetite except the Orange site, which is the only location to have no magnetite present at all. Site F3 has a higher Ms value than the rest of the Lake Cowal sites (F1-F6) due to anomalously higher concentrations of magnetite. There is no known cause for greater amounts of magnetite. It is not present at those concentrations upwind, nor is it likely to come from the gold mine. While industrial sources such as vehicle exhaust and brake pads can contribute magnetite to the surroundings, site F3 is over two miles distant from the mine entrance, farther than sites F1 and F2 which did not show anomalous Ms values.

HIRM measurements show relative contributions of high and low coercivity minerals, which can be useful in determining dust provenance. However, fields used to measure HIRM are only as high as 1T, which does not saturate either the goethite or hematite, leading to underestimated contributions. Moreover, there is no distinction in these measurements between the goethite

and hematite components, rendering the results incomplete and useful only to estimate relatively high or low contributions.

There was an unexpected amount of variability between the HIRM results due to measurement noise in IRM_{1T} and IRM_{-300} measurements. While each measurement itself matched USGS measurements within error, once the two large numbers were subtracted and divided, the error compounded to cause the variation we observed.

The L-ratio presented by Liu et. al. (2007) was designed to test if HIRM is dependent on hematite concentration alone or also influenced by unconventional coercivity due fine grain sizes or isomorphic substitution. Figure 4-1 shows HIRM vs. L-ratio. The broad liner relationship between L-ratio and HIRM

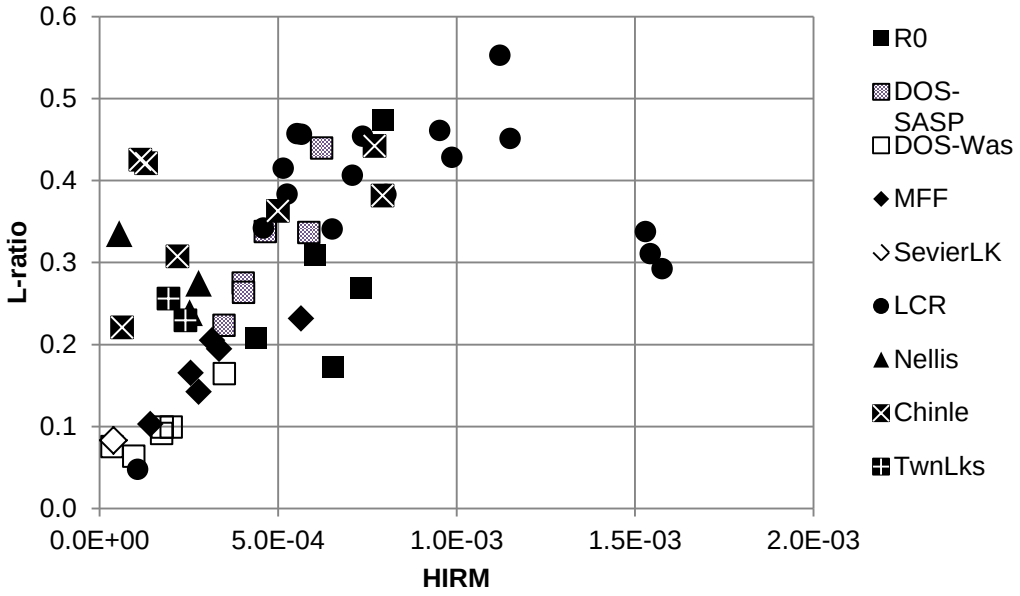

Figure 4-1: L-ratio vs. HIRM

suggests a coercivity dependence, therefore L-ratio is not independent of HIRM and is somewhat affected by grain size or isomorphic substitution.

Mössbauer results indicate that the majority of magnetic components at room temperature are hematite particles. This only takes into account grains that are blocked at room temperature, discounting the SP grain size range. Section 4.4 will compare the results of HIRM with hematite components measured by Mössbauer and goethite tests.

The Guyodo goethite test showed that all natural samples had a goethite component along with both a high and low coercivity component attributed to hematite and magnetite/maghemite. Despite not being able to calculate actual weight percentages, it is clear that there must be a much greater amount of hematite and goethite than magnetite in order for the two weakly magnetic minerals to even be detected. This is most true in the case of goethite.

4.2 Grain Size

Grain size is determined through multiple methods. Some experiments only determine relative amounts of particular grain size fractions or grain sizes of particular coercivities. By comparing grain size analysis methods, a better understanding of overall contributions can be observed. Many grain size indicators such as hysteresis properties, ARM, and SIRM use low strength fields

that measure only low coercivity magnetite and maghemite concentrations, whereas Mössbauer spectroscopy and low temperature remanence can detect the fine grained behavior of high coercivity hematite and goethite.

ARM and SIRM ratios are used to determine the grain size of low coercivity minerals like magnetite. Samples that have a higher SD-PSD concentration will yield higher ARM/SIRM values. Combined with Xfd%, which shows relative SP contribution, ARM/SIRM ratios will show relative mixtures of grain sizes (Figure 4-2). Samples that plot higher on the y-axis have more SD concentrations while those appearing lower have a greater MD concentration. Distance across the x-axis shows increasing SP contribution.

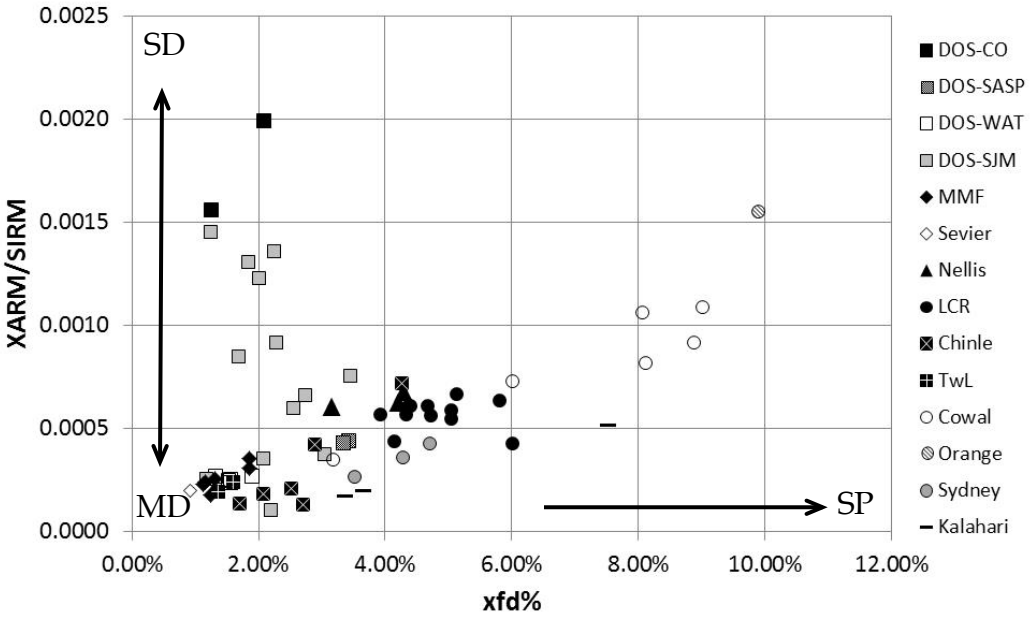

Figure 4-2: XARM/SIRM vs. Xfd% shows grain size abundances. Samples higher on the y-axis have greater SD contributions while lower samples have more MD contribution. Several locations including LCR, Chinle, and CO-DOS show clear groupings indicating similar grain size components.

The Day plot (Day, 1977) compares the ratios of hysteresis parameters Br, Bcr, Mr and Ms to determine domain states of grains and, therefore, relative grain size. Figure 4-3 shows the Day plot of American southwest samples and Red Dawn Australian samples with SP-SD and SD-MD mixture trendlines. According to the Day plot, grain size increases to the lower right of the plot while fine grains group in the upper left. The American southwest dust samples fall mostly in the middle under the pseudo single domain range with LCR samples towards the finer side. Twin Lakes samples are the exception, plotting in the multi-domain range. Dunlop (2002) found that PSD grains tend to be mixtures of MD and SD grains. His trendlines shown in the figure reflect mixing lines for synthetic magnetite grains. The Day Plot is a measure of mostly the ferrimagnetic magnetite fraction; however, high coercivity contribution can be observed as samples that plot above the trendlines.

Australian dust from Lake Cowal is on the finer side while there is a distinct increase in grain size within the city of Sydney. Although this would seem to imply a trend towards increasing grain size as locations go downwind, it is more likely that industrial pollutants are contributing the MD grains due to the proximity of the sites with coarsest grains to local sources of pollution such as the Cowal Gold Mine or the city of Sydney. This is supported by the unexpectedly coarse size at site F1, which is located adjacent to the mine entrance.

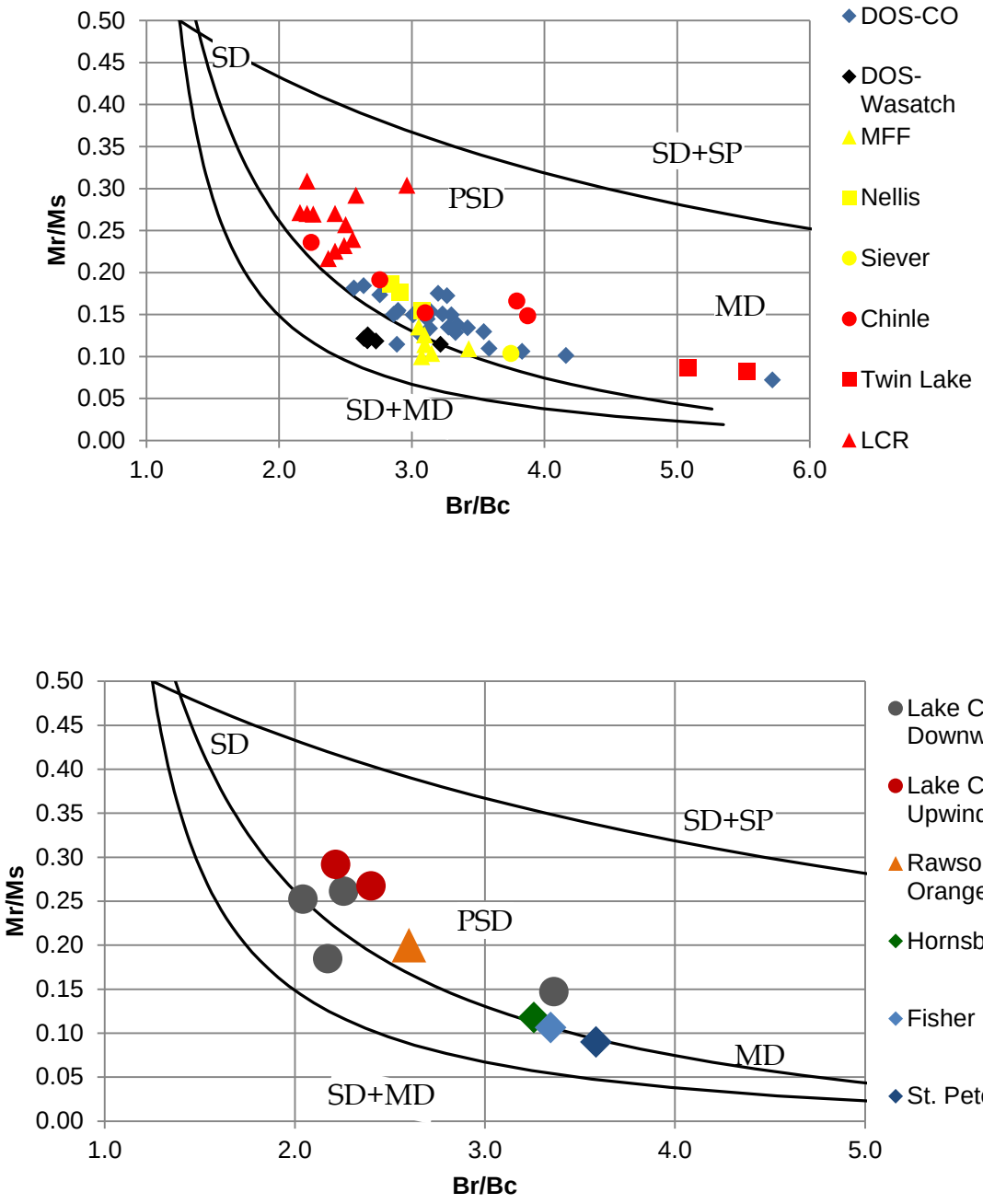

Figure 4-3: Day Plot with SP-SD and SD-MD mixing curves. Grain size gets larger towards the lower right and smaller towards the upper left.

Mössbauer spectroscopy is not inherently used to determine grain size, however, because samples could be measured at both 300 K and 4.2 K, a comparison of contribution by component can be made in order to determine the changes due to SP grain sizes that are unblocked at room temperature but become blocked at low temperature, increasing mineral percentages. The difference in percentage between 4.2 K and 300 K reflect percent SP contribution. This value is particularly high in the goethite fraction, which is not detected by Mössbauer measurements at all at room temperature but shows great gains at 4.2 K, indicating that the majority of the goethite in samples is nano size.

Another sign of nano particles is suppression of low temperature transitions. Many natural samples demonstrated breaks in slope on cooling and warming during the Guyodo goethite test after AF demagnetization that are thought to be Morin transitions suppressed by 50-100 K. Such transition temperature suppression is only found in very fine grains. Özdemir et. al. (2008) found that T_M was only significantly suppressed in grain sizes between 30-90 nm. These findings close to the findings of this study's synthetic samples. The 25nm nanohematite sample shows a highly suppressed Morin transition between 150-170 K, approximately 100 K lower than that expected from a bulk sample.

Additionally, the suppressed Morin transitions show thermal hysteresis, in which T_M varies from cooling to warming cycles. Özdemir et. al. (2008) posited that thermal hysteresis was due to crystal imperfections or a broad range of grain

sizes. In this study, samples with suppressed Morin transitions are thought to be in the 30-90 nm size range, limiting the range of grain sizes and pointing to crystal imperfections as the cause of the thermal hysteresis.

The last examination of grain size comes from two samples sieved to multiple sizes. One sample from the Little Colorado River, Tucker Flat 3, was sieved to three different particle sizes (63, 20, and 10 um), which were all measured to examine how decreasing grain size affects magnetic properties of natural samples. Additionally, one other sample, Tyende Court- Stop 15, was also measured at 20 and 10 um. Ms changed slightly as can be seen from the slope-corrected hysteresis loops (Figure 4-4). Oddly, Ms decreased in Tucker Flat 3 at size PM 10 and increased at smaller size for Tyende Court. No significant changes in hysteresis properties were observed. The Guyodo goethite test showed different amounts of remanence attributed to goethite lost on thermal demagnetization (Figure 4-5), but the difference totals only 0.74% of the total magnetization. No significant differences were observed in low temperature transitions, which occur at approximately 180 K and are attributed to the hematite Morin transition. Perhaps significant changes were not found between the different particle sizes because all the sizes were tens of microns. Even at sizes of 10 um, most iron oxide grains are MD.

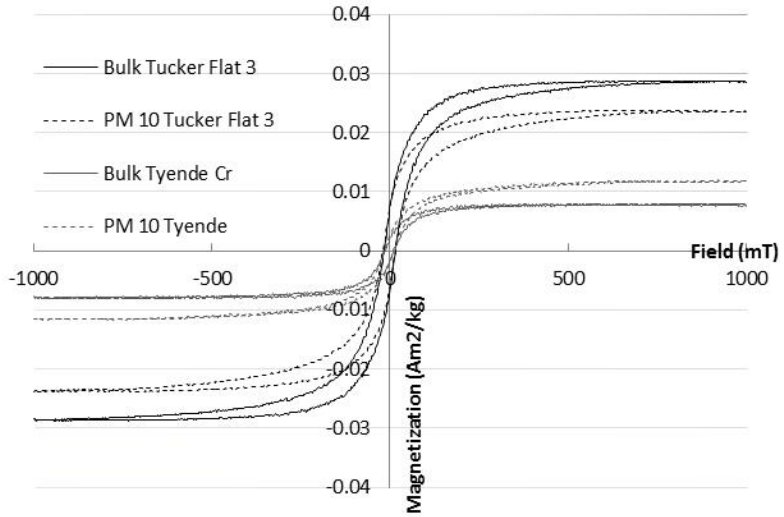

Figure 4-4: Slope Corrected Hysteresis Loops. Samples Tyende Court and Tucker Flat 3 shown at 20 um (solid lines) and 10 um (dashed lines).

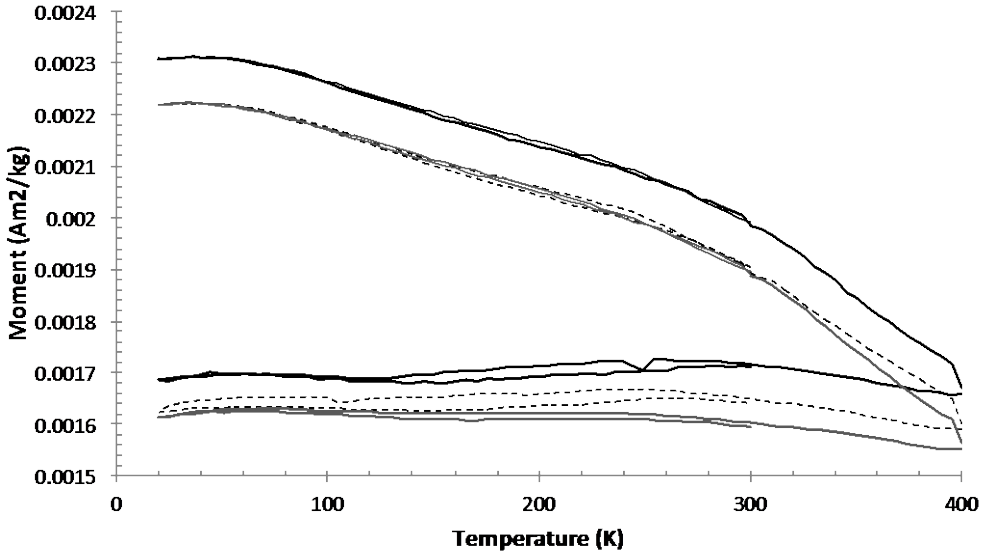

Figure 4-5: Goethite test after AF demagnetization showing three different grain sizes. The dashed line shows the remanence measured on the 63 um grain size. The gray line represents <20 um and the black line is PM 10.

4.3 Goethite Tests

4.3.1 Maher Test

The Maher goethite test uses very high fields to isolate the moment due to goethite. Goethite alone continues to increase in remanence at fields greater than 3 T while the acquisition curve of hematite levels off by around 2.5 T. Maher's method saturates all of the magnetite and the majority of the hematite in a 2 T field and measures the sample's remanence on cooling and warming. It then goes on to magnetize the sample further to 5 T and repeat the cooling and warming curve. The change in remanence from 2 T to 5 T is due almost entirely to goethite.

In addition to the change in moment, the Maher test shows changes in slope on cooling and warming between each step. As the goethite fraction becomes more magnetized, the slope becomes steeper. When hematite is present, the Morin Transition causes a decrease in remanence, resulting in a lower slope than there would be otherwise. Synthetic hematite standards have remanence that decreases as temperature lowers, resulting in positive slopes. To a limited extent, samples high in goethite have more highly negative slopes while samples with less goethite have flatter slopes. Therefore, slope is a good indicator of the qualitative amount of goethite. A caveat to this distinction is factoring in other minerals. A synthetic maghemite standard showed an even

greater negative slope which, taken alone, would have appeared like goethite. However, the maghemite also had a wide gap between cooling and warming curves and displayed a break in slope that would indicate the presence of magnetite by the Verwey transition. A large negative slope with these other factors would be unlikely to be mistaken for goethite yet it is not clear how mixed components affect slope.

It would not be expected that a change in field strength in the Maher test would influence transition temperatures for any mineral. In every natural sample, T_V did not change as field strength increased except in synthetic maghemite in which there was a marked change in T_V from 110 K at 2 T to 120-121 K at 5 T. This change in T_V only occurred in one sample, making it unclear as to whether this was a coincidence or error from machine noise.

4.3.2 Guyodo Test

The Guyodo goethite test is important because it can distinguish the three main components and provide the magnetic moments attributed to each. It does not, however, allow all weight percentages to be calculated because the saturation magnetization for the mineral goethite is poorly known and is a strong function of impurities, particle size, and crystallinity. Without Ms, the weight percent of goethite would be greatly underestimated. Likewise, there are

many assumptions that need to be made about hematite in order to calculate weight percent such that accurate figures are unlikely to be produced. Calculating weight percent assumes that all grains are SD in size and blocked at room temperature. No nano-sized grains would be taken into account and therefore percentages would be underestimated. Hematite would also have to be chemically pure with little isomorphic substitution, which is rare in natural samples. Lastly, the calculations would assume that there are no other minerals present with high coercivity such as perhaps oxidized maghemite grains.

The warming and cooling curves at each step of the goethite test contribute useful information. The first step after imparting a 2.5 T field shows the Verwey transition if present. At this stage, magnetite overpowers the other iron oxide minerals. After AF demagnetization, however, the Verwey transition disappears and the curves display a negative slope from the monotonic increase of the goethite signal. The curve is not completely linear due to the magnetic signatures of other minerals present. Morin transitions can be prominent at this step, depending on the size of the hematite. Almost without fail, any Morin transition will also show thermal hysteresis with a slightly lower T_M on cooling. On cooling and warming, T_M is suppressed to temperatures well below 260 K. In the final cooling and warming curve after thermal demagnetization of goethite, the Morin transition becomes more prominent and the slope of the curve becomes less negative. Theoretically all that remains magnetized in this final

stage is high coercivity minerals, namely hematite. While the slope of the curves levels off, however, it does not completely disappear. This residual slope could be due to a small amount of goethite not being demagnetized at 400 K. Perhaps grain defects or isomorphic substitution prevent certain grains from demagnetizing at the Curie temperature. Lack of total demagnetization of goethite up to 400 K would result in goethite concentrations being underestimated.

4.3.3 Guyodo-Lascu Test

The Guyodo-Lascu test was made to measure the change in moment on thermal demagnetization of goethite at 400 K, without the AF demagnetization step. Bypassing the low field demagnetization step allowed a continuous measurement, uninterrupted by offline treatment by the user. The amount of goethite was determined by the percentage of remanence that was lost during thermal demagnetization up to 400 K. Because of the low fields used in the Guyodo-Lascu test, hematite was hardly magnetized and even magnetite was undersaturated, allowing an alternate way of measuring the goethite without being overpowered. Normally, any goethite would remain unaffected by such a low field but by combining the low field with cooling through the Curie temperature, goethite holds a small remanence. The percentages of goethite in

the Guyodo-Lascu test were consistently higher than the original Guyodo test. This finding is likely due to the way the percentages are counted out of the total magnetization. In the Guyodo-Lascu test, hematite is largely untouched by the magnetic field, meaning that the goethite signal accounts for more of the total magnetization.

There was a question of how the AF demagnetizing field affects fine-grained goethite on the SP/SD boundary. To exam this uncertainty, the measurement of one sample was altered in the Guyodo-Lascu test to include an AF demagnetizing field prior to thermal demagnetization of goethite. If small AF demagnetizing fields affect only magnetite with no effect on goethite, we would expect the decrease in moment on thermal demagnetization to stay the same from one test to the next. There was, however, an order of magnitude decrease in the amount of remanence attributed to goethite during heating to 400 K using the altered Guyodo-Lascu test, indicating that AF fields, even at low magnitude, influenced goethite content. Small demagnetization fields may cause the amount of goethite in a sample, particularly fine-grained particles, to be underestimated.

The Guyodo-Lascu test further examined fine-grains with blocking temperatures between 200 and 300 K. By magnetizing grains in a field below room temperature, a greater portion of grains may carry remanence. Grains that were on the SP/SD boundary are exposed to fields as they lose thermal energy

and become ordered, locking the magnetic moment in and raising the overall magnetic moment of the sample. The difference in moment between the 200 K and 300 K steps is due solely to fine-grained particles that order just below room temperature.

Despite a small to no amount of hematite being magnetized by the Guyodo-Lascu test, synthetic nanohematite does appear to become magnetized. This is likely because the entire sample is hematite, and the instrument sensitivity is delicate enough to detect the low amount of hematite, unlike natural samples in which magnetic minerals are a small fraction of the whole.

4.4 Comparing Mineral Compositions Among Methods

While the goethite test provides a telling differentiation between iron oxide minerals, it does not magnetize the finer fraction of unblocked grains, which likely make up a greater part of the distribution of grain sizes. Mössbauer measurements, on the other hand, detect all iron molecules contained in the sample regardless of size but are less sensitive than magnetic measurements, unable to confidently detect less than 2 wt% concentration. Importantly, Mössbauer spectra, unlike the goethite test, can be measured at room temperature or low temperature, revealing more iron oxide minerals that magnetically order below 300 K. Because fine-grained particles often make up

the bulk of the iron distribution in atmospheric dust (Lawrence et. al., 2010), they are an important component of the samples. The percentages produced by the Mössbauer spectra show percent of the total magnetic fraction, rather than a specific weight percent. A pure hematite sample and a natural sample with only hematite iron oxide in an otherwise paramagnetic bulk mixture would both produce outcomes of 100% hematite.

All of the measurements carried out by this study analyzed the bulk sample, rather than the surface minerals. While this can often be a desirable trait, in the context of solar reflectivity on snow, the surfaces of particles are the most important. Reflectivity studies previously carried out by the USGS did measure surfaces alone, however, instrument sensitivity was not as precise as magnetic studies. Library indices of minerals, particularly those in the nano size range, were also slim, making reflectivity findings less reliable.

Each of the goethite tests magnetizes different fractions of minerals at different field intensities, making them difficult to compare. However, there are positive correlations between increases in mineral content measured among HIRM, Mössbauer, and Goethite tests. There is a positive correlation between percentages found for magnetite and hematite compared to SIRM and HIRM values respectively (Figure 4-7). There is likewise a positive correlation between HIRM and percent hematite measured by Mössbauer (Figure 4-6). There does

not seem to be any correlation between percentages found from the goethite test compared to coercivity unmixing.

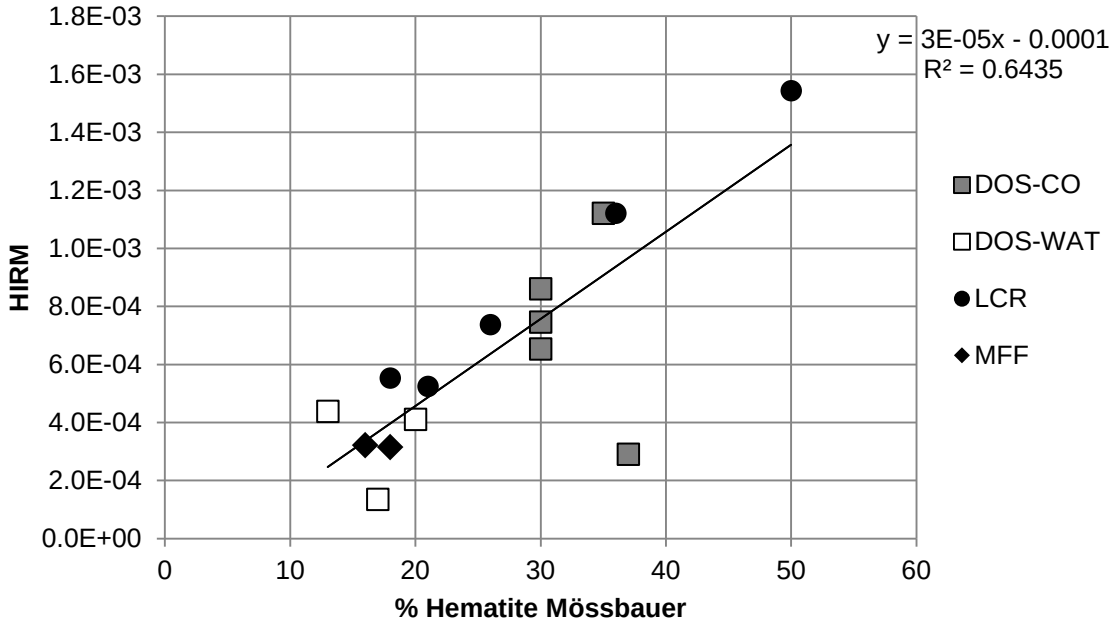

Figure 4-6: HIRM vs % Hematite from Mössbauer measurements. There is a linear trend between values representing quantity of hematite in samples.

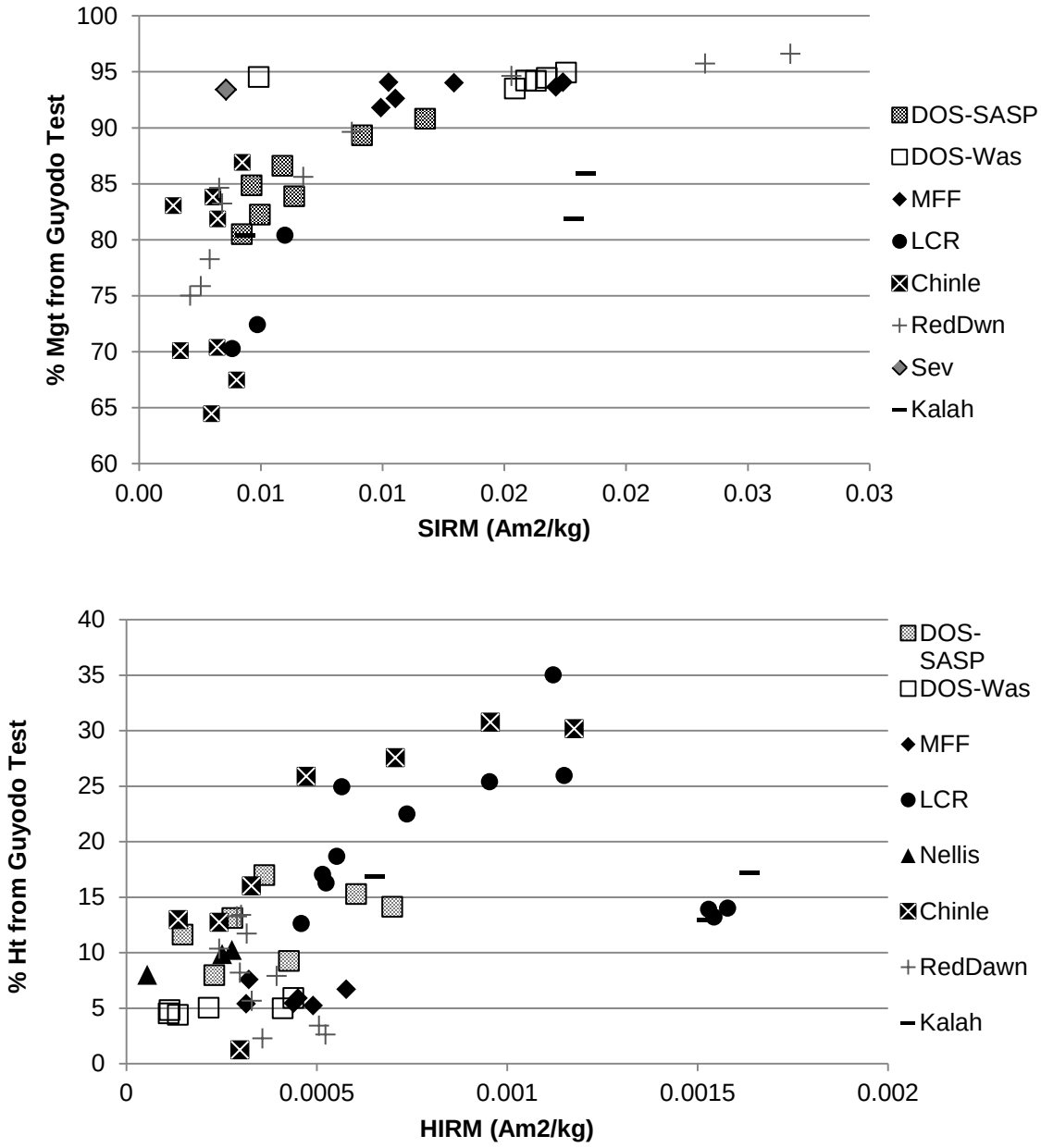

Figure 4-7: SIRM vs. % Magnetite and HRIM vs. % Hematite from Goethite Test.

The 5T field of the Maher test does not seem to obtain moments that are as high as goethite tests that utilize lower fields (see Figure 4-8). Perhaps this is because the grains are not cooled in a field through their blocking

temperature(s). This would significantly make a difference in how we test for goethite in the future because it could indicate that pulsing samples to high fields such as 9 T would not be as effective as heating samples through 400 K.

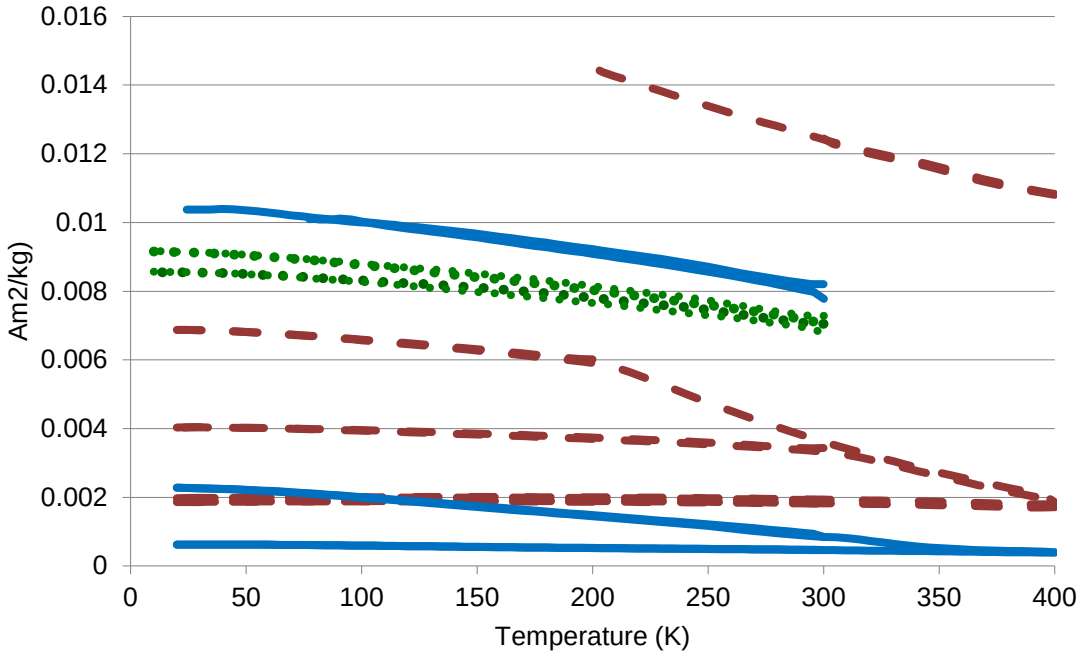

Figure 4-8: All three goethite tests shown for sample Orange from the Red Dawn dust storm in Australia. Dashed is Lascu test. Solid is Guyodo. Dotted is Maher test. Remanence measured by Maher test at 5 T is lower than that of the Guyodo test at only 2.5 T.

4.5 Coercivity Unmixing

All the samples that were measured for the coercivity unmixing program fit best with three components that possibly correlate to magnetite, hematite, and goethite. Egli (2004) found that atmospheric samples usually had little skewness. The components were therefore fit using as little skewness as possible while still

providing a good fit. The components' coercivity distributions did not overlap extensively, a factor that indicates distinct solutions that more accurately reflect the data. Figure 4-9 shows sites F1-F6 near the Cowal gold mine. The amplitude reflects percent contribution of a particular component. Site F3 seems anomalous. Samples from F3 have higher amplitudes of low coercivity minerals, which is in agreement with higher Ms values at that site. Similarly, coercivity unmixing shows similar trends in site F6 located in the agricultural fields upwind of the gold mine. Site F6, however, does not have high Ms values. It is possible that F3 has a higher percentage of magnetite from industrial sources (machinery exhaust or mine pollution), except that by that explanation, site F1, located adjacent to the main entrance would be expected to have similar amounts of magnetite as well. There could be a low coercivity material being carried between sites F3 and F6. However it is unlikely that magnetite would be lower upwind as magnetite content tends to decrease with distance traveled.

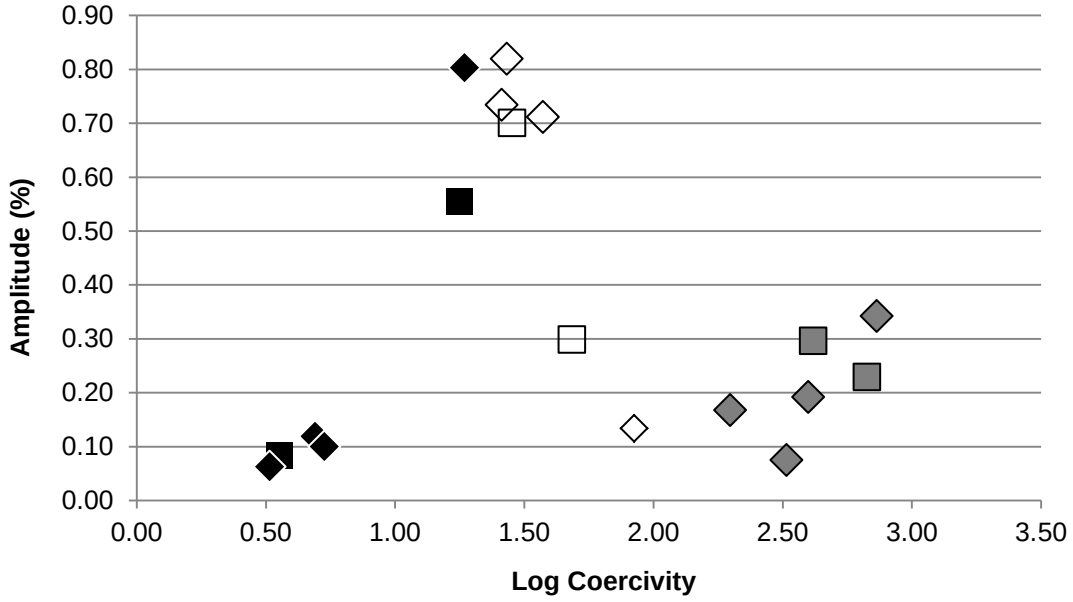

Figure 4-9: Amplitude vs. Log Coercivity. Black shapes represent the lowest coercivity component, while white shapes and gray shapes correspond to components two and three, respectively. Diamonds are sites downwind from the Cowal Gold Mine and squares are upwind.

4.6 High Field Acquisition

The high field acquisition in natural samples did not show the expected results at fields above 5 T. As fields approached 5 T and beyond, rather than becoming saturated, samples lost remanence. It would be expected that samples with only low coercivity components would quickly reach saturation at which point acquisition would discontinue, leaving a flat slope. Instead, samples would seem to peak and then drop to a lower moment, despite multiple exposures to high fields. The same drop in remanence by the same amount

appears when samples are reversed and acquisition is applied in the backwards direction.

Conversely, the synthetic mineral standards seem to acquire remanence as expected. Even the most pure standards, however, contain traces of other minerals. For example, the 10x100 nm goethite standard seems to acquire remanence up to 600 mT and then level off until fields of 2.5-3 T (See Figure 4-10). The WS222 standard, composed mostly of goethite, acquires remanence at much lower fields than expected, which also indicates hematite contamination of the sample. Because there seems to be no irregularity with the synthetic samples, the oddity of losing remanence at high fields seems to be a product of the natural samples themselves.

There was a loss in saturation moment of the nano-sized standards and several Bodele samples over the course of two weeks. Sometimes measurements even minutes apart could show a drop in the moment. The decrease in remanence is likely due to viscous decay, which is not unexpected in a grain size so small. Thermal fluctuations give the grains enough energy to overcome energy barriers and seek lower energy states along easy axes so that they slowly demagnetize simply by being at room temperature. What this indicates is that any values regarding the percentage of remanence contributed at high fields is a minimum estimation.

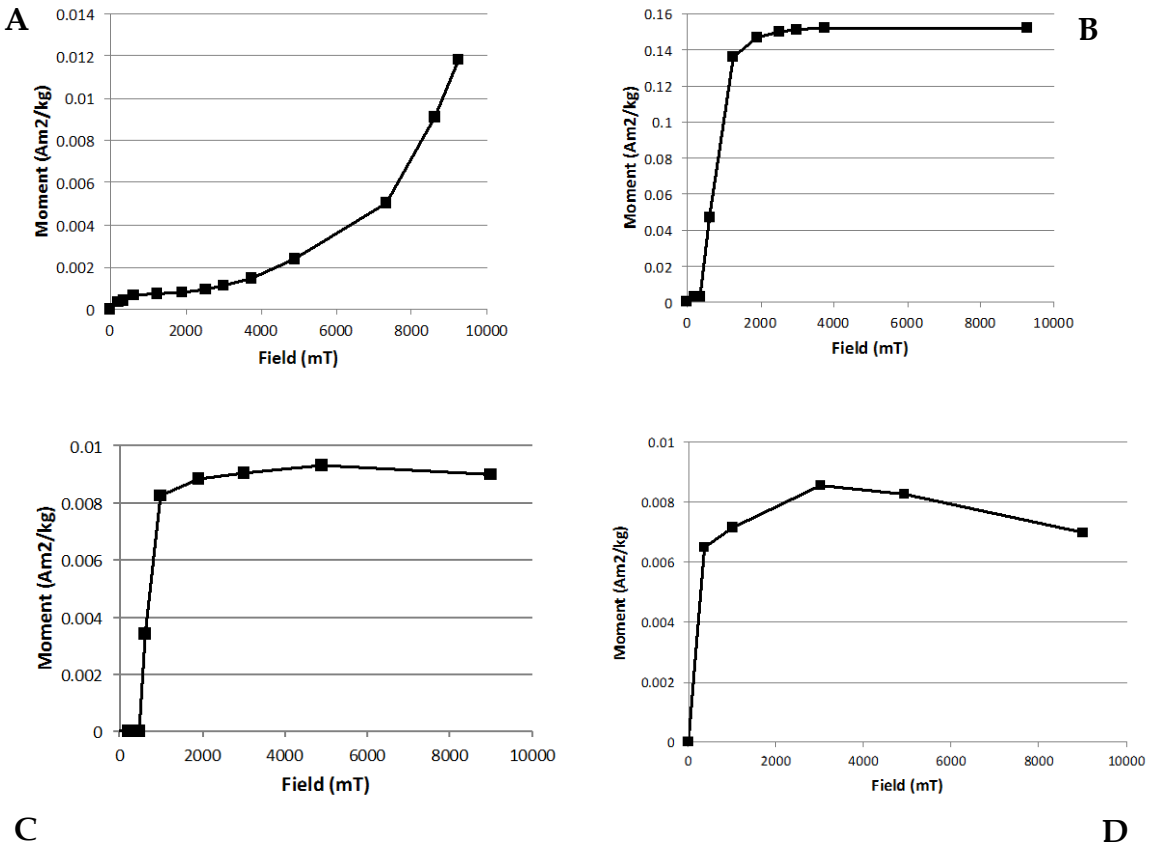

Figure 4-10: High field acquisition curves. A) Goethite 10x100 nm standard acquisition. It is evident that lower coercivity minerals saturate resulting in a flattened slope at 2 T before goethite acquisition takes over and remanence sharply rises. At 9T, there is no sign of saturation. B) Skyspring hematite standard. There appears to be a small terrace point at low fields (220-360 mT) that represents the saturation of magnetite contamination. Hematite is mostly saturated between 2-2.5 T. C) Orange sample with no magnetite component and almost no remanence until fields of 475 mT. Remanence sharply increases and is nearly saturated by 2 T. D) Sample CH2-63um from Bodele shows greatest gain in remanence between 0-360 mT due to low coercivity magnetite and continued acquisition between 360-3000 mT due to hematite. This sample shows loss of remanence at very high fields.

Pulsing the 10x100 nm goethite standard multiple times at 9.2T at first appeared to cause steady increase in moment but after repeating the experiment at 9T, the finding could not be duplicated. A magnetic pulse so close to the coil capacity is likely less accurate, resulting in fluctuating fields. In natural samples

with significant ferrimagnetic component, this would likely go unnoticed but for goethite alone, a small change at high field results in large changes of the proportion magnetized.

4.7 Dust Sourcing

While hematite and goethite are important for their radiative characteristics in absorbing solar radiation, magnetite is an important mineral for tracing source material in dust. The Ms of MFF and Wasatch are much higher than the rest of the American southwest samples, which likely indicates more magnetite. These two sites also have higher SIRM values, which supports the finding. Sigma values are negative for most of MFF, Sevier Lake, and Wasatch samples. Negative sigma hysteresis is not seen anywhere else in the American southwest dust except for one R0 sample. Sigma values that stray from zero can be indications of SP contributions or changes in oxidation state (Fabian, 2003). However, the negative sigma values are so close to zero that these Utah samples are not significantly telling. Figure 4-11 shows sigma values plotted against Ms. An inverse relationship seems to be present so that as Ms (and low coercivity minerals) decreases, sigma becomes more wasp-waisted (positive). Perhaps this only shows that certain locations have very little variation in Ms and sigma and therefore have one single source of each mineral component while other

locations may plot broadly have multiple mineral components or distinct grain sizes.

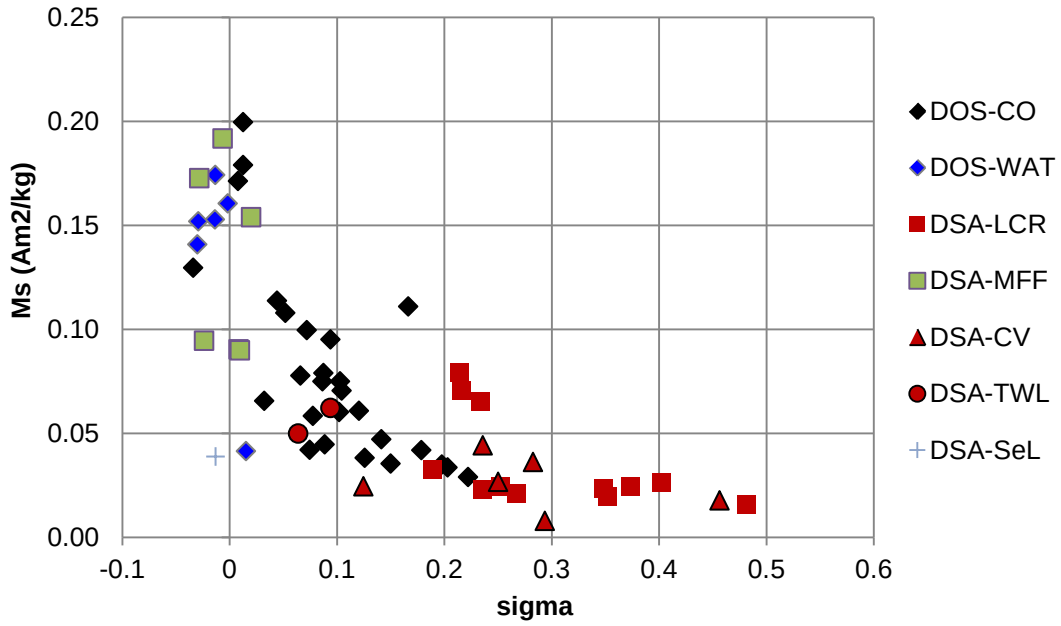

Figure 4-11: Sigma vs. Ms. DSA samples from Utah plot very closely with the Wasatch DOS While DSA from Arizona and New Mexico have higher sigma and therefore more SP contribution. Colorado DOS has a broad range of values that indicate multiple sources.

Plotting SIRM vs. HIRM values for DOS and DSA samples show correlations between quantities of hematite and magnetite. Higher HIRM and SIRM values indicate higher concentrations of hematite and magnetite, respectively. Figure 4-12 and Figure 4-13 show DSA samples plotted with Wasatch and Colorado DOS respectively with a dashed line indicating the transition between low and high levels of hematite. Wasatch DOS samples tend to have high levels of magnetite but low hematite while Colorado DOS sites have

a range of hematite and relatively low magnetite. Like the Wasatch DOS, MFF samples have high magnetite and relatively low hematite whereas LCR and Chinle Valley samples have low magnetite and a range of hematite that is more similar to the Colorado DOS.

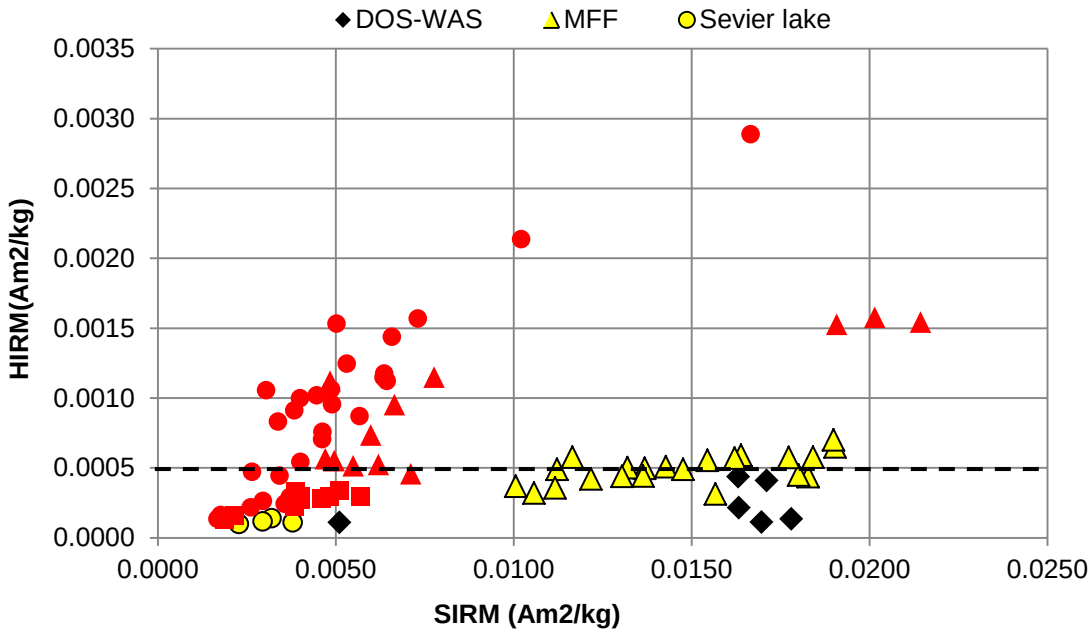

Figure 4-12: HIRM vs. SIRM. The Wasatch DOS has low HIRM values corresponding to lower levels of hematite, which is similar to MFF DSA samples and unlike LCR, Chinle Valley and Twin Lakes samples.

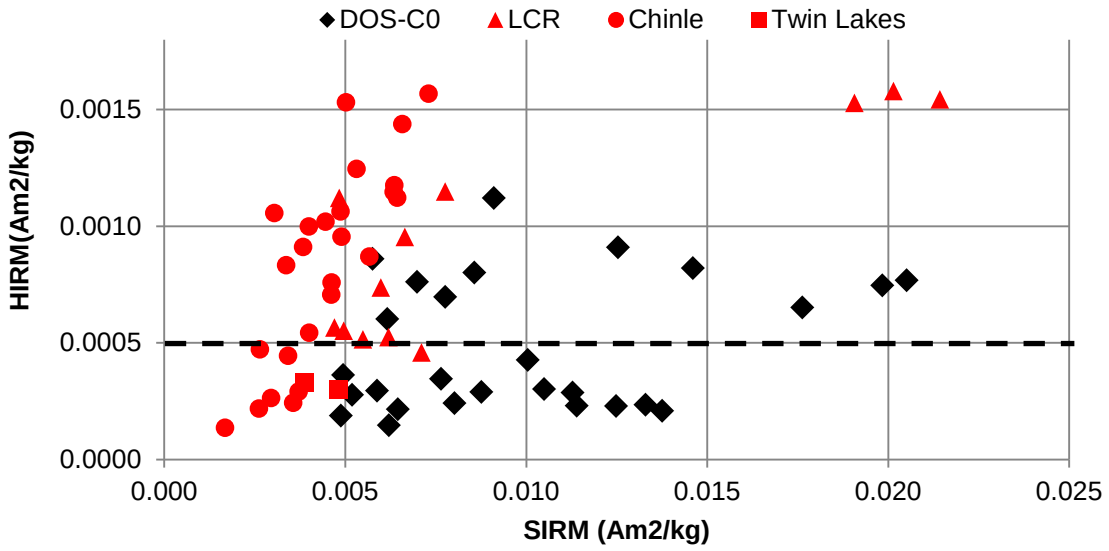

Figure 4-13: Colorado HIRM vs. SIRM. Colorado DOS does not have as high levels of magnetite but has a range of hematite values similar to the LCR and Chinle Valley sites.

5 Conclusions

5.1 Composition

The goethite test and reflectance spectroscopy measurements show that the majority of the magnetic minerals in the natural dust samples are composed of combinations of hematite and goethite minerals. Many samples contain magnetite as well but at small fractions of a weight percent not detectable by non-magnetic methods. There was good coordination between the weight percent of hematite calculated from the Guyodo goethite test, HIRM measurements, and Mössbauer spectroscopy, but the trend lines are not one to one. This could be due to the different sizes and coercivities measured due to the field strength used, temperatures at which measurements were carried out, and machine sensitivity. Goethite did not apparently get magnetized in HIRM measurements due to field strengths of only 1 T. There was no correlation between percent goethite from the Guyodo test and HIRM. Likewise, it was rare to detect any goethite in Mössbauer measurements at room temperature. The goethite tests seem to be one of the only effective ways of measuring goethite. The MagMix coercivity unmixing program fit each distribution curve to three components, likely corresponding to magnetite, hematite, and goethite. However, the measurements would need a better signal-to-noise ratio in order to discern possible minerals from multiple sources. Because component amplitudes

share little correlation with percentages from other methods, it is unclear how accurately the coercivity unmixing reflects true values.

5.2 Grain Size

The hematite and goethite that appears in the natural samples is greatly composed of nano-sized particles. There was consistently evidence of nano particles in multiple measurements including Mössbauer with increases of goethite at low temperature, in goethite tests in cooling and warming curves with suppressed Morin transitions, and in the increase in remanence at 200 K in the Guyodo-Lascu goethite test. Magnetite grains, however, appear to be coarser based on hysteresis parameters.

5.3 Goethite Tests

Each goethite method is good at showing a part of the picture. The standard Guyodo test is still the most robust measurement because it imparts a thermal magnetization to goethite and measures cooling and warming curves of each of the three major components. However, it only magnetizes grains blocked at 300 K. The Lascu-Guyodo test magnetizes a greater portion of grains on cooling from 400 to 200 K but does not provide information about hematite and very little on magnetite due to the low field applied. The Maher test only focuses

on goethite, which, while useful, does not include a thermal magnetization step and can result in lower remanence. The thermal magnetization of grains through the Curie temperature significantly makes a difference in remanence imparted.

5.4 High field IRM Acquisition

Most of the natural samples lose remanence when saturation would be expected. Decreases in remanence seem to be inherent in the sample and are repeatable on acquisition in the backwards direction. It is unclear if this behavior is in fact due to aspects of the sample or to machine error but evidence points to the former. Synthetic iron oxide samples acquire remanence well and do not show decreases in remanence at high fields. IRM acquisition in these samples shows impurities very well.

5.5 Dust Sourcing

MFF and Wasatch dust have many similarities including high Ms values, slightly negative sigma hysteresis, relatively low levels of high coercivity minerals, and similar groupings when comparing hysteresis properties, xfd%, and ARM and SIRM ratios which all measure primarily the low coercivity magnetite component. Unlike Wasatch samples, SASP-DOS, Chinle Valley, and

LCR samples have more variability in hematite content and have few low coercivity minerals grains like magnetite.

5.6 Future Work

The goal of studying atmospheric dust in the American southwest is to fit more accurate numbers to climate modeling parameters so that well-informed decisions can be made regarding water resource regulation in the Colorado River Basin and so remediation efforts can be carried out to prevent wind sediment erosion of the Colorado Plateau. Taking into account the number of observed dust storms along with wind direction and known parent sediment mineral composition could lead to more accurate albedo models which would allow for advance warning of peak snow melt times and allow for water from the Upper Colorado River Basin to be moved to the lower basin and free reservoirs for extra springtime melt.

It is certain that continuing atmospheric dust studies will focus on higher fields to better characterize the goethite components of samples. More samples will be collected, particularly after known dust storm events. There will also be a need to characterize more synthetic dust standards of the nano scale in order to examine in greater detail the nuances of such small particle sizes. Additionally, a greater array of sampling locations around the world will round out global dust

inventories and provide more comprehensive information about dust patterns moving on a larger scale.

At the Institute for Rock Magnetism, more measurements will be taken. Mössbauer spectroscopy has not been completed at room and low temperatures. Likewise, the Lascu and Maher goethite tests can be carried out on further samples. The 9 T pulse magnetometer will be useful in multiple applications for future measurements. For instance, using the three-step high field acquisition in conjunction with the Maher test could give results that could be used in the parameters H_{cool} and H_{cool}% set forth by Maher et. al. (2004).

Finding a better way to magnetize a greater portion of the distribution of grain sizes would be useful. Perhaps a greater percentage of goethite could be magnetized in the goethite tests if higher fields were used. A combination of cooling through the Curie temperature in a high (2.5 to 5 T) field followed by offline exposure to a 9 T field pulse would magnetize a greater portion of the goethite distribution.

More samples need to be measured using the altered Lascu test with the AF demagnetization step in order to determine whether small AF fields affect very fine grain goethite. If this is the case, another modification of the Guyodo test could be implemented to retain the full goethite magnetization. By switching the order of demagnetization steps, goethite grains could be thermally demagnetized before partial AF demagnetization. Demagnetizing goethite first would ensure

that there would be a low chance that any other steps would interfere with goethite grains. In doing so, comparisons between the two tests could be made to determine the very fine-grained fraction that is lost in small alternating fields.

6 References:

Alfaro, S. C. (2004). Iron oxides and light absorption by pure desert dust: An experimental study. *Journal of Geophysical Research*, *109*(D8), D08208. doi:10.1029/2003JD004374

Anderson, K. A., & Downing, J. A. (2006). Dry and wet atmospheric deposition of nitrogen , phosphorus and silicon in an agricultural region. *Water, Air, and Soil Pollution*, *176*, 351–374. doi:10.1007/s11270-006-9172-4

Aragón, R., Buttrey,D.J., Shepherd, J.P., & Honig J.M. (1985). Influence of nonstoichiometry on the Verwey transition *Phys. Rev. B.*, 31, 430–436.

Bando, Y., Kiyama, M., Yamamoto, N., Takada, T., Shinjo, T., Takaki, H. (1965). The magnetic properties of α-Fe_2O_3 fine particles, *J. Phys. Soc. Japan* 20, 2085.

Banerjee, S. K. (1971). New grain size limits for paleomagnetic stability in haematite. *Nature Physical Science*, *232*, 15–16.

Brand, R.A. (1987). Improving the validity of hyperfine field distributions from metallic alloys. Part I: Unpolarized source. Nuclear Instruments and Methods in Physics Research B, v. 28, p. 398-405.

Butler, R. F., & Banerjee, S. K. (1975). Theoretical single-domain grain size range in magnetite and titanomagnetite. *Journal of Geophysical Research*, *80*(29), 4049–4058. doi:10.1029/JB080i029p04049

Cattle, S.R., Hemi, K, Pearson G.L., and Sanderson, T. (2012)Distinguishing and characterising point-source mining dust and diffuse-source dust deposits in a semi-arid district of eastern Australia, Aeolian Research 6, 21–29

Chevallier, R., Mathieu, S. (1943). Proprietes magnetiques des poudres d'hematite-influence des dimensions des grains. *Annales Phys.*, 18, 258–288.

Day, R., Fuller, M., and Schmidt, V. A. (1977). Hysteresis properties of titanomagnetites: grain size and composition dependence, *Phys. Earth Planet, inter.,* 13, 260-267.

Dekkers, M.J. (1989). Magnetic properties of natural goethite: II. TRM behavior during thermal and alternating field demagnetization and low temperature treatment, *Journal of Geophysical Research,* 97, 323–340.

Dunlop, D.J. (1972). Magnetite: behavior near the single-domain threshold, *Science*, 176(4030), 41-43.

Dunlop, D. J. (1973). Superparamagnetic and single-domain threshold sizes in magnetite. *Journal of Geophysical Research*, *78*(11), 1780–1793. doi:10.1029/JB078i011p01780

Dunlop, D. J. (2002). Theory and application of the Day plot (Mrs/Ms versus Hcr/Hc). *Journal of Geophysical Research, 107*(B3), 1–22.

Egli, R. (2004). Characterization of individual rock magnetic components by analysis of remanence curves, 1. Unmixing natural sediments. *Studia Geophysica et Geodaetica*, *48*(2), 391–446. doi:10.1023/B:SGEG.0000020839.45304.6d

Engelbrecht, J.P. and Derbyshire, E. (2010). Airborne mineral dust. *Elements* 6(4), 241-246. Doi:10.2113/gselements.6.4.241

Evans, M.E., Heller, F. (2003). *Environmental Magnetism: Principles and Applications of Enviromagneitcs*, Academic Press. 299 pp.

Fabian, K. (2003). Some additional parameters to estimate domain state from isothermal magnetization measurements. *Earth and Planetary Science Letters*, *213*(3-4), 337–345. doi:10.1016/S0012-821X(03)00329-7

France, D. E., & Oldfield, F. (2000). Identifying goethite and hematite from rock magnetic measurements of soils and sediments. *Journal of Geophysical Research*, *105*, 2781–2795.

Galloway, J. N., Thornton, J. D., Norton, S. A., Volchok, H. L., & McLean, R. A. N. (1982). Trace metals in atmospheric deposition: A review and assessment. *Atmospheric Environment (1967)*, *16*(7), 1677–1700. doi:10.1016/0004-6981(82)90262-1

Gassó, S., Grassian, V.H., and Miller, R.L. (2010). Interactions between Mineral Dust, Climate, and Ocean Ecosystems. *Elements*. 6(4), 247-252. doi: 10.2113/gselements.6.4.247

Guyodo, Y., LaPara, T. M., Anschutz, A. J., Penn, R. L., Banerjee, S. K., Geiss, C. E., & Zanner, W. (2006). Rock magnetic, chemical and bacterial community analysis of a modern soil from Nebraska. *Earth and Planetary Science Letters*, *251*(1-2), 168–178. doi:10.1016/j.epsl.2006.09.005

Haigh, G. (1957). Observations on the magnetic transition of hematite at -15° C. *Philosophical Magazine*, 2(19) 877-890.

Kneller, E. F., & Luborsky, F. E. (1963). Particle size dependence of coercivity and remanence of single-domain particles. *Journal of Applied Physics*, *34*(3), 656. doi:10.1063/1.1729324

Lascu, I., & Feinberg, J. M. (2011). Speleothem magnetism. *Quaternary Science Reviews*, *30*(23-24), 3306–3320. doi:10.1016/j.quascirev.2011.08.004

Lawrence, C. R., Painter, T. H., Landry, C. C., & Neff, J. C. (2010). Contemporary geochemical composition and flux of aeolian dust to the San Juan Mountains, Colorado, United States. *Journal of Geophysical Research*, *115*(G3), G03007. doi:10.1029/2009JG001077

Leys, J.F., Heidenreich, S.K., Strong, C.L., McTainsh, G.H., Quigley, S. (2011). PM10 concentrations and mass transport during "Red Dawn" – Sydney 23 September 2009. *Aeolian Res*. 3, 327–342.

Liu, Q., Roberts, A. P., Torrent, J., Horng, C.-S., & Larrasoaña, J. C. (2007). What do the HIRM and S -ratio really measure in environmental magnetism? *Geochemistry Geophysics Geosystems*, *8*(9). doi:10.1029/2007GC001717

Maher, B. a., Karloukovski, V. V., & Mutch, T. J. (2004). High-field remanence properties of synthetic and natural submicrometre haematites and goethites: significance for environmental contexts. *Earth and Planetary Science Letters*, *226*(3-4), 491–505. doi:10.1016/j.epsl.2004.05.042

McNab, T.K., Fox, R.A., Boyle, A.J.F. (1968). Some magnetic properties of magnetite (Fe_3O_4) microcrystals. *J. Appl. Phys,* 39, 5703-5711.

Morin, F. J. (1950), Magnetic susceptibility of α-Fe_2O_3 and α-Fe_2O_3 with added titanium, *Phys. Rev.*, 78, 819–820, doi:10.1103/PhysRev.78.819.2.

Moskowitz, B. M., Jackson, M., & Kissel, C. (1998). Low-temperature magnetic behavior of titanomagnetites. *Earth and Planetary Science Letters*, *157*(3-4), 141–149. doi:10.1016/S0012-821X(98)00033-8

Neél, L. (1947). Propriétés d'un ferromagnétique cubique en grain fins. *C. R. Acad. Sci. Paris,* 224, 1488-1490.

Özdemir, Ö., & Dunlop, D. J. (1999). Low-temperature properties of a single crystal of magnetite oriented along principal magnetic axes. *Earth and Planetary Science Letters*, *165*, 229–239.

Özdemir, Ö., Dunlop, D. J., & Berquó, T. S. (2008). Morin transition in hematite: Size dependence and thermal hysteresis. *Geochemistry Geophysics Geosystems*, *9*(10). doi:10.1029/2008GC002110

Painter, T. H., Barrett, A. P., Landry, C. C., Neff, J. C., Cassidy, M. P., Lawrence, C. R., McBride, K. E., et al. (2007). Impact of disturbed desert soils on duration of mountain snow cover. *Geophysical Research Letters*, *34*(12), L12502. doi:10.1029/2007GL030284

Painter, T. H., Deems, J. S., Belnap, J., Hamlet, A. F., Landry, C. C., & Udall, B. (2010). Response of Colorado River runoff to dust radiative forcing in snow. *Proceedings of the National Academy of Sciences of the United States of America*, *107*(40), 17125–30. doi:10.1073/pnas.0913139107

Plumlee, G.S., and Ziegler, T.L. (2003). The medical geochemistry of dusts, soils, and other earth materials. *Treatise on Geochemistry*, v.9, edted by B. S. Lollar, p.263-310, Elsevier, New York.

Rochette, P& Fillion, G. (1989). Field and temperature behavior of remanence in synthetic goethite: paleomagnetic implications. *Geophysical Research Letters*, *16*(8), 851–854.

Rochette, P., Mathé, P.-E., Esteban, L., Rakoto, H., Bouchez, J.-L., Liu, Q., & Torrent, J. (2005). Non-saturation of the defect moment of goethite and fine-grained hematite up to 57 Teslas. *Geophysical Research Letters*, *32*(22), L22309. doi:10.1029/2005GL024196

Schwertmann, U., Taylor, R.M. (1989). Iron Oxides. In: Dixon, J.B. and Weed, S.B. {eds.} Minerals in soils environments {2nd ed.}. Soil Sci. Soc. Am. Book Series No. 1, Madison, WI, 379-438.

Stacey, F.D. (1962). A generalized theory of thermoremanence, covering the transition from single domain to multi-domain magnetic grains, *Philosophical Magazine,* 7(83) pp?

7 Appendix

Table 7-1: Complete Hysteresis Properties

Sample	Location	Ms (Am^2/kg)	Mr (Am^2/kg)	Bc (mT)	Bcr (mT)
SASP D2-WY10	DOS-SASP	0.0419	0.0076	12.53	32.13
SASP D6-WY10	DOS-SASP	0.0350	0.0061	12.90	35.60
SASP D4WY11	DOS-SASP	0.03818	0.005699	10.70	33.3325
SASP D5WY11	DOS-SASP	0.095	0.014	9.97	30.01
SASP D6WY11	DOS-SASP	0.036	0.005	11.10	34.84
SASP D7WY11	DOS-SASP	0.061	0.008	9.39	33.26
SASP D8WY11	DOS-SASP	0.071	0.011	10.66	30.81
Wasatch Bulk	DOS-Was	0.1650	0.0175	7.09	22.90
Lower Red Pine	DOS-Was	0.1529	0.0182	8.80	23.47
Upper Red Pine	DOS-Was	0.1605	0.0195	8.79	23.20
Upper Mill B	DOS-Was	0.1518	0.0174	9.36	30.10
Lower Mill B	DOS-Was	0.1742	0.0207	8.80	23.46
Blind Hollow	DOS-Was	0.1408	0.0177	10.35	27.63
SOLA	DOS-Was	0.0415	0.0049	9.31	25.42
9254	MFF	0.1538	0.0159	7.91	24.92
09296	MFF	0.0904	0.0103	9.48	29.39
09308	MFF	0.0945	0.0119	9.05	28.04
09365	MFF	0.1726	0.0172	9.08	27.92
09383	MFF	0.1918	0.0210	8.01	27.47
10470	MFF	0.0899	0.0121	9.83	30.01
JY09-01A	Sevier Lake	0.0389	0.0040	7.38	27.66
Bridsprings 3	LRC, AZ	0.0328	7.104E-03	14.73	34.94
Dinnebito Wash	LRC	0.0229	6.200E-03	16.46	35.53
Hwy 2 Playa Edge	LRC	0.0266	7.761E-03	17.54	45.27

Mud Lk LowerCr	LRC	0.0652	2.015E-02	19.28	42.61
Mud Lk Up Loose	LRC	0.0795	2.143E-02	16.51	37.29
Mud Lake Up Defl	LRC	0.0705	1.907E-02	17.13	37.90
Road6732 Playa N	LRC	0.0233	5.983E-03	16.14	40.39
Road6732 Playa S	LRC	0.0197	4.707E-03	14.82	37.88
Toolani Lake West	LRC	0.0214	4.960E-03	15.00	37.36
Toolani Lk West 2	LRC	0.0244	5.487E-03	14.76	35.77
Tucker Flat	LRC	0.0159	4.840E-03	20.76	61.51
Tucker Flat 3	LRC	0.0246	6.650E-03	17.10	41.41
Dinnebito <63um	LRC	0.0395	0.0076	12.69	42.0606
Rd6732 N <63um	LRC	0.0290	0.0065	12.71	39.4546
ToolaniLkW <63um	LRC	0.0499	0.0083	10.67	36.2307
Tucker Fl 3 <63um	LRC	0.0289	0.0071	15.56	45.2134
PM10 Tucker Flat 3	LRC	0.0237	0.0067	17.30	44.6486
Nellis 2.2	Nelis, NV	0.0057	8.735E-04	11.56	35.5405
Nellis 3.1	Nelis	0.0328	5.807E-03	12.01	34.9068
Nellis 3.2	Nelis	0.0302	5.616E-03	13.01	37.0038
PM 10 Tyende Cr.	Chinle Valley	0.011624	0.0021	12.34	29.0691
Stop 15 Tyende Cr	Chinle	0.0080	0.0019	12.90	28.92
Stop 23 - TPW	Chinle	0.0267	0.0051	13.42	37.02
NN110314-2	Chinle	0.0178	0.0029	7.87	13.67
NN110314-6	Chinle	0.0442	0.0066	12.63	47.89
NN110315-2	Chinle	0.0362	0.0055	11.81	45.76
NN110315-8	Chinle	0.0246	0.0040	10.16	31.53
NN110316-2	Twin Lakes	0.0622	0.0054	6.91	35.12
NN110316-6	Twin Lakes	0.0500	0.0041	5.35	29.56
BK1	Kalahari	0.1044	0.0225	15.22	33.01
GB1	Kalahari	0.0268	0.0059	15.64	39.43
SZ1	Kalahari	0.0969	0.0229	15.46	

F1	Australia	0.0196	0.0029	13.82	46.46
F2	Australia	0.0131	0.0034	14.32	32.32
F3	Australia	0.0407	0.0075	9.72	21.13
F4	Australia	0.0149	0.0038	12.73	26.01
F5	Australia	0.0096	0.0026	16.18	38.84
F6	Australia	0.0116	0.0034	14.57	32.28
Fisher	Australia	0.2482	0.0263	9.02	30.20
Hornsby	Australia	0.1258	0.0148	8.00	26.07
Orange	Australia	0.0521	0.0104	7.02	18.26
StPeters	Australia	0.2633	0.0236	5.98	21.43
Nano-Goethite	(10x100nm)	0.0023	0.0003	33.89	164.52
Nano-Hematite	(25nm)	0.1985	0.0500	48.26	108.43
Alpha Fe2O3	(Skyspring)	0.2053	0.0836	69.20	130.39
Gamma Fe2O3	(Skyspring)	61.51	12.41	10.23	17.25
GDS27	(USGS)	0.2614	0.1357	140.88	240.51
WS222	(USGS)	0.0370	0.0067	70.02	385.92
CH8_125-2000	Bodele	0.0082	9.75E-05	1.08	21.57
CH11_125-2000	Bodele	0.0042	0.0006	11.43	31.06
CH80_125-2000	Bodele	0.0025	0.0004	10.38	30.78
CH81_125-2000	Bodele	0.0027	0.0005	11.35	31.50
CH62_It63	Bodele	0.0045	0.0007	16.06	39.61
CH39_It63	Bodele	0.5196	0.0959	10.38	22.61
CH2_It63	Bodele	0.0324	0.0055	11.31	31.78
CH11_It63	Bodele	0.0153	0.0036	14.92	41.82
CH24_It63	Bodele	0.0022	0.0005	6.39	32.51
CH23_It63	Bodele	0.0049	0.0009	6.71	24.93
CH80_It63	Bodele	0.0289	0.0055	12.97	39.20
CH81_It63	Bodele	0.0218	0.0040	12.85	38.62
CH8_It63	Bodele	0.0169	0.0034	13.67	39.04

Table 7-2: Complete Susceptibility Results

Sample	Location	Xac 1Hz	Xac 1000 Hz	X'' 1 Hz	Xhf	Xf	Xfd%
SASP D2-WY10	DOS-SASP	0.042	7.60E-03	12.53	4.98E-08	4.64E-07	32.10
SASP D6-WY10	DOS-SASP	0.035	6.10E-03	12.90	4.61E-08	3.79E-07	35.60
SASP D4WY11	DOS-SASP	0.038	5.70E-03	10.70	4.79E-08	3.80E-07	33.30
SASP D5WY11	DOS-SASP	0.095	1.40E-02	9.97	5.63E-08	9.48E-07	30.00
SASP D6WY11	DOS-SASP	0.036	5.00E-03	11.10	3.55E-08	3.11E-07	34.80
SASP D7WY11	DOS-SASP	0.061	8.00E-03	9.39	3.48E-08	5.39E-07	33.30
SASP D8WY11	DOS-SASP	0.071	1.10E-02	10.66	5.11E-08	6.56E-07	30.80
Wasatch Bulk	DOS-Wasatch	0.165	1.75E-02	7.09	5.03E-08	1.37E-06	22.90
Lower Red Pine	DOS-Wasatch	0.153	1.82E-02	8.80	5.00E-08	1.50E-06	23.47
Upper Red Pine	DOS-Wasatch	0.161	1.95E-02	8.79	5.37E-08	1.43E-06	23.20
Upper Mill B	DOS-Wasatch	0.152	1.74E-02	9.36	5.15E-08	1.37E-06	30.10
Lower Mill B	DOS-Wasatch	0.174	2.07E-02	8.80	5.16E-08	1.50E-06	23.46
Blind Hollow	DOS-Wasatch	0.141	1.77E-02	10.35	4.63E-08	1.15E-06	27.63
SOLA	DOS-Wasatch	0.042	4.90E-03	9.31	4.51E-08	3.89E-07	25.42
9254	MFF	0.154	1.59E-02	7.91	5.12E-08	1.36E-06	24.92
09296	MFF	0.090	1.03E-02	9.48	3.49E-08	7.41E-07	29.39
09308	MFF	0.095	1.19E-02	9.05	4.56E-08	9.37E-07	28.04
09365	MFF	0.173	1.72E-02	9.08	4.45E-08	1.47E-06	27.92
09383	MFF	0.192	2.10E-02	8.01	3.93E-08	1.60E-06	27.47

10470	MFF	0.090	1.21E-02	9.83	5.35E-08	8.28E-07	30.01
JY09-01A	Sevier Lake	0.039	4.00E-03	7.38	1.06E-08	2.78E-07	27.66
Bridsprings 3	LRC, AZ	0.033	7.10E-03	14.73	6.17E-08	3.40E-07	34.94
Dinnebito Wash	LRC	0.023	6.20E-03	16.46	7.09E-08	2.95E-07	35.53
Hwy 2 Playa Edge	LRC	0.027	7.76E-03	17.54	7.87E-08	3.56E-07	45.27
Mud Lk LowerCr	LRC	0.065	2.02E-02	19.28	5.76E-08	8.56E-07	42.61
Mud Lk Up Loose	LRC	0.080	2.14E-02	16.51	5.58E-08	1.06E-06	37.29
Mud Lk Up Defl	LRC	0.071	1.91E-02	17.13	5.94E-08	9.91E-07	37.90
Road6732 Playa N	LRC	0.023	5.98E-03	16.14	7.33E-08	2.94E-07	40.39
Road6732 Playa S	LRC	0.020	4.71E-03	14.82	6.44E-08	2.51E-07	37.88
Toolani Lk W	LRC	0.021	4.96E-03	15.00	7.56E-08	2.60E-07	37.36
Toolani Lk West 2	LRC	0.024	5.49E-03	14.76	7.79E-08	2.95E-07	35.77
Tucker Flat	LRC	0.016	4.84E-03	20.76	8.17E-08	1.92E-07	61.51
Tucker Flat 3	LRC	0.025	6.65E-03	17.10	7.27E-08	2.39E-07	41.41
Dinnebito <63um	LRC	0.040	7.60E-03	12.69	6.31E-08	4.02E-07	42.06
Rd6732 N <63um	LRC	0.029	6.50E-03	12.71	7.63E-08	3.39E-07	39.45
Tool LkW <63um	LRC	0.050	8.30E-03	10.67	5.66E-08	4.91E-07	36.23
Tucker Fl 3 <63um	LRC	0.029	7.10E-03	15.56	7.16E-08	3.23E-07	45.21
PM10 Tucker Fl 3	LRC	0.024	6.70E-03	17.30	7.83E-08	3.48E-07	44.65
Nellis 2.2	Nelis, NV	0.006	8.74E-04	11.56	4.64E-08	6.06E-08	35.54
Nellis 3.1	Nelis	0.033	5.81E-03	12.01	7.08E-08	4.18E-07	34.91

Nellis 3.2	Nelis	0.030	5.62E-03	13.01	5.42E-08	3.61E-07	37.00
PM 10 Tyende Cr.	Chinle	0.012	2.10E-03	12.34	5.87E-08	1.29E-07	29.07
Stop 15 Tyende Cr	Chinle	0.008	1.90E-03	12.90	5.84E-08	9.55E-08	28.92
Stop 23 - TPW	Chinle	0.027	5.10E-03	13.42	3.05E-08	2.36E-07	37.02
NN110314-2	Chinle	0.018	2.90E-03	7.87	2.29E-08	1.59E-07	13.67
NN110314-6	Chinle	0.044	6.60E-03	12.63	2.96E-08	3.58E-07	47.89
NN110315-2	Chinle	0.036	5.50E-03	11.81	4.90E-08	2.80E-07	45.76
NN110315-8	Chinle	0.025	4.00E-03	10.16	6.09E-08	1.72E-07	31.53
NN110316-2	Twin Lakes	0.062	5.40E-03	6.91	7.06E-08	4.21E-07	35.12
NN110316-6	Twin Lakes	0.050	4.10E-03	5.35	3.11E-08	5.02E-07	29.56
BK1	Kalahari	0.104	2.25E-02	15.22	6.12E-08	8.90E-07	33.01
GB1	Kalahari	0.027	5.90E-03	15.64	4.48E-08	4.57E-07	39.43
SZ1	Kalahari	0.097	2.29E-02	15.46	7.34E-08	3.21E-07	
F1	Australia	0.020	2.90E-03	13.82	7.61E-08	1.65E-07	46.46
F2	Australia	0.013	3.40E-03	14.32	7.04E-08	2.06E-07	32.32
F3	Australia	0.041	7.50E-03	9.72	7.58E-08	7.52E-07	21.13
F4	Australia	0.015	3.80E-03	12.73	6.27E-08	2.91E-07	26.01
F5	Australia	0.010	2.60E-03	16.18	6.80E-08	1.22E-07	38.84
F6	Australia	0.012	3.40E-03	14.57	6.80E-08	2.02E-07	32.28
Fisher	Australia	0.248	2.63E-02	9.02	6.22E-08	2.50E-06	30.20
Hornsby	Australia	0.126	1.48E-02	8.00	9.01E-08	1.82E-06	26.07

Orange	Australia	0.052	1.04E-02	7.02	1.02E-07	1.95E-06	18.26
StPeters	Australia	0.263	2.36E-02	5.98	7.45E-08	2.66E-06	21.43
Nano-Goethite	(10x100nm)	2.30E-03	3.00E-04	33.89	3.79E-07	-1.35E-08	164.52
Nano-Hematite	(25nm)	0.199	5.00E-02	48.26	2.49E-07	5.98E-07	108.43
Alpha Fe2O3	(Skyspring)	0.205	8.36E-02	69.20	3.03E-07	7.64E-07	130.39
Gamma Fe2O3	(Skyspring)	61.510	1.24E+01	10.23	2.48E-06	5.19E-04	17.25
GDS27	(USGS)	0.261	1.36E-01	140.88	2.01E-07	3.77E-07	240.51
WS222	(USGS)	0.037	6.70E-03	70.02	3.17E-07	-1.75E-07	385.92
CH8_125-2000	Bodele	8.20E-03	9.75E-05	1.08	5.58E-08	2.39E-08	21.57
CH11_125-2000	Bodele	4.20E-03	6.00E-04	11.43	8.34E-08	3.09E-08	31.06
CH80_125-2000	Bodele	2.50E-03	4.00E-04	10.38	7.13E-08	1.93E-08	30.78
CH81_125-2000	Bodele	2.70E-03	5.00E-04	11.35	8.57E-08	2.45E-08	31.50
CH62_It63	Bodele	4.50E-03	7.00E-04	16.06	1.02E-07	3.92E-08	39.61
CH39_It63	Bodele	0.520	9.59E-02	10.38	1.23E-07	5.19E-06	22.61
CH2_It63	Bodele	0.032	5.50E-03	11.31	3.09E-08	2.82E-07	31.78
CH11_It63	Bodele	0.015	3.60E-03	14.92	3.11E-08	1.58E-07	41.82
CH24_It63	Bodele	2.20E-03	5.00E-04	6.39	8.73E-08	1.42E-08	32.51
CH23_It63	Bodele	4.90E-03	9.00E-04	6.71	4.61E-08	5.16E-08	24.93
CH80_It63	Bodele	0.029	5.50E-03	12.97	5.12E-08	2.85E-07	39.20
CH81_It63	Bodele	0.022	4.00E-03	12.85	4.72E-08	2.08E-07	38.62
CH8_It63	Bodele	0.017	3.40E-03	13.67	2.80E-08	1.85E-07	39.04

Table 7-3: Complete Guyodo Goethite Test Results*

Sample	Location	Magnetite (Am^2/kg)	Hematite (Am^2/kg)	Goethite (Am^2/kg)	Total Magn.	% Mgt	% Ht	% Gt
SASP D2-WY10	DOS-SASP	6.28E-03	1.06E-03	1.47E-04	7.48E-03	83.88	14.16	1.96
SASP D6-WY10	DOS-SASP	5.20E-03	9.68E-04	1.55E-04	6.33E-03	82.24	15.30	2.46
SASP D4WY11	DOS-SASP	4.49E-03	6.95E-04	1.06E-04	5.29E-03	84.86	13.14	2.00
SASP D5WY11	DOS-SASP	1.14E-02	1.00E-03	1.49E-04	1.26E-02	90.82	8.00	1.18
SASP D6WY11	DOS-SASP	3.99E-03	8.42E-04	1.24E-04	4.95E-03	80.51	17.00	2.49
SASP D7WY11	DOS-SASP	5.89E-03	7.91E-04	1.18E-04	6.80E-03	86.62	11.64	1.74
SASP D8WY11	DOS-SASP	8.56E-03	8.89E-04	1.33E-04	9.59E-03	89.34	9.27	1.39
Wasatch Bulk	DOS-Was	1.32E-02	5.84E-04	1.02E-04	1.39E-02	95.08	4.19	0.73
Lower Red Pine	DOS-Was	1.41E-02	8.97E-04	8.37E-05	1.51E-02	93.51	5.94	0.55
Upper Red Pine	DOS-Was	1.61E-02	8.22E-04	1.17E-04	1.70E-02	94.47	4.84	0.69
Upper Mill B	DOS-Was	1.52E-02	8.16E-04	1.14E-04	1.61E-02	94.24	5.05	0.70
Lower Mill B	DOS-Was	1.41E-02	7.45E-04	1.20E-04	1.49E-02	94.20	4.99	0.80
Blind Hollow	DOS-Was	1.67E-02	7.76E-04	1.14E-04	1.76E-02	94.93	4.41	0.65
SOLA	DOS-Was	4.63E-03	2.22E-04	4.53E-05	4.90E-03	94.54	4.54	0.92
09254	MFF	1.35E-02	7.73E-04	8.20E-05	1.43E-02	94.03	5.40	0.57
09296	MFF	7.68E-03	6.35E-04	5.11E-05	8.37E-03	91.80	7.59	0.61
09308	MFF	9.68E-03	7.00E-04	7.18E-05	1.05E-02	92.61	6.70	0.69
09365	MFF	1.55E-02	8.95E-04	7.85E-05	1.64E-02	94.08	5.45	0.48

09383	MFF	1.51E-02	9.56E-04	7.18E-05	1.62E-02	93.64	5.91	0.44
10470	MFF	9.49E-03	5.28E-04	6.96E-05	1.01E-02	94.07	5.24	0.69
JY09-01A	Sevier Lake	3.11E-03	2.02E-04	1.74E-05	3.33E-03	93.42	6.06	0.52
Bridsprings 3	LRC, AZ	5.64E-03	8.45E-04	2.06E-04	6.69E-03	84.30	12.62	3.08
Dinnebito Wash	LRC	4.54E-03	9.09E-04	1.39E-04	5.59E-03	81.23	16.27	2.49
Hwy 2 Playa Edge	LRC	5.10E-03	1.90E-03	3.34E-04	7.33E-03	69.48	25.96	4.55
Mud Lk LowerCr	LRC	1.58E-02	2.64E-03	4.18E-04	1.88E-02	83.77	14.01	2.22
Mud Lk Up Loose	LRC	1.51E-02	2.37E-03	4.20E-04	1.79E-02	84.45	13.21	2.34
Mud Lake Up Defl	LRC	1.44E-02	2.41E-03	4.93E-04	1.73E-02	83.24	13.91	2.85
Road6732 Playa N	LRC	4.32E-03	1.31E-03	1.80E-04	5.81E-03	74.39	22.50	3.11
Road6732 Playa S	LRC	3.30E-03	1.13E-03	1.18E-04	4.55E-03	72.46	24.94	2.60
Toolani Lake West	LRC	3.75E-03	9.04E-04	1.89E-04	4.84E-03	77.41	18.68	3.91
Toolani Lk West 2	LRC	4.23E-03	9.08E-04	1.84E-04	5.32E-03	79.48	17.07	3.46
Tucker Flat	LRC	2.80E-03	1.70E-03	3.63E-04	4.86E-03	57.52	35.02	7.46
Tucker Flat 3	LRC	4.39E-03	1.59E-03	2.94E-04	6.28E-03	69.92	25.39	4.69
Rd6732 N <63um	LRC	2.89E-03	9.97E-04	1.04E-04	3.99E-03	72.41	24.98	2.61
ToolaniLkW <63um	LRC	6.06E-03	1.31E-03	1.69E-04	7.54E-03	80.42	17.34	2.24
Tucker Fl 3 <63um	LRC	4.47E-03	1.64E-03	2.51E-04	6.36E-03	70.27	25.77	3.95
PM10 Tucker Flat 3	LRC	4.80E-03	1.71E-03	2.75E-04	6.78E-03	70.72	25.23	4.05

Nellis 2.2	Nelis, NV	7.03E-04	6.34E-05	2.33E-05	7.90E-04	89.02	8.03	2.95
Nellis 3.1	Nelis	4.85E-03	5.72E-04	1.59E-04	5.59E-03	86.91	10.25	2.84
Nellis 3.2	Nelis	4.47E-03	5.09E-04	1.72E-04	5.15E-03	86.76	9.89	3.35
PM 10 Tyende Cr.	Chinle Valley	-	-	-	-	-	-	-
Stop 15 Tyende Cr	Chinle	1.44E-03	2.25E-04	6.86E-05	1.73E-03	83.06	12.98	3.96
Stop 23 - TPW	Chinle	2.95E-03	1.16E-03	8.52E-05	4.19E-03	70.40	27.57	2.03
NN110314-2	Chinle	2.42E-03	8.92E-04	1.39E-04	3.45E-03	70.10	25.88	4.02
NN110314-6	Chinle	4.14E-03	1.85E-03	1.44E-04	6.13E-03	67.47	30.18	2.35
NN110315-2	Chinle	3.15E-03	1.50E-03	2.34E-04	4.89E-03	64.47	30.75	4.78
NN110315-8	Chinle	2.90E-03	4.40E-04	1.19E-04	3.46E-03	83.81	12.74	3.44
NN110316-2	Twin Lakes	3.77E-03	5.36E-05	5.14E-04	4.33E-03	86.90	1.24	11.87
NN110316-6	Twin Lakes	2.98E-03	5.83E-04	7.67E-05	3.64E-03	81.86	16.03	2.11
BK1	Kalahari	1.54E-02	2.32E-03	2.06E-04	1.80E-02	85.91	12.94	1.15
GB1	Kalahari	3.79E-03	7.95E-04	1.32E-04	4.72E-03	80.37	16.84	2.79
SZ1	Kalahari	1.33E-02	2.81E-03	1.56E-04	1.63E-02	81.82	17.22	0.96
F1	Australia	2.57E-03	4.54E-04	3.64E-04	3.39E-03	75.84	13.41	10.75
F2	Australia	2.77E-03	2.68E-04	2.35E-04	3.27E-03	84.62	8.19	7.19
F3	Australia	5.35E-03	4.95E-04	4.04E-04	6.25E-03	85.61	7.92	6.47
F4	Australia	2.48E-03	3.09E-04	1.91E-04	2.98E-03	83.23	10.36	6.40
F5	Australia	2.45E-03	4.33E-04	3.83E-04	3.27E-03	75.01	13.26	11.73
F6	Australia	2.56E-03	3.83E-04	3.28E-04	3.27E-03	78.26	11.72	10.02

Fisher	Australia	2.03E-02	4.78E-04	2.35E-04	2.10E-02	96.61	2.27	1.12
Hornsby	Australia	1.28E-02	4.65E-04	2.64E-04	1.35E-02	94.62	3.43	1.95
Orange	Australia	7.36E-03	4.66E-04	3.85E-04	8.21E-03	89.63	5.68	4.69
StPeters	Australia	1.93E-02	5.33E-04	3.30E-04	2.02E-02	95.73	2.64	1.63
Nano-Goethite	(10x100nm)	2.00E-03	1.26E-05	2.04E-02	2.24E-02	8.90	0.06	91.05
Nano-Hematite	(25nm)	1.71E-02	3.15E-02	7.22E-03	5.58E-02	30.62	56.45	12.93
Alpha Fe2O3	(Skyspring)	3.98E-02	2.92E-02	2.68E-02	9.59E-02	41.55	30.50	27.95
Gamma Fe2O3	(Skyspring)	7.32E+00	-	< 0.00174	-	-	-	-
GDS27	(USGS)	1.38E-01	2.39E-02	1.12E-02	1.73E-01	79.71	13.82	6.47
WS222	(USGS)	2.23E-03	2.23E-03	2.87E-02	3.31E-02	6.73	6.73	86.54

*The goethite tests were not measured on the Bodele samples.